# Immunogenicity and Structure of stabilized HIV-1 Clade-C Env from pediatric Elite-neutralizer complexed with autologous bNAb

Swarandeep Singh[1,†], Sanjeev Kumar[1,2,†], Arnab Chatterjee[3,†], Lakshay Malhotra[4], Muneeb Pervez[1], Abdul Rahman[1], Ifrah Andrabi[1], Bapan Mondal[3], Sanket Katpara[1], Shaifali Sharma[1], Harsh Bhakri[1], Anjli Gaur[1], Tanu Bansal[1], Vikram Iyer[1], Abdul Wahid Hussain[1], Shubbir Ahmed[6], Rajesh Kumar[5], Ethayathulla Abdul Samath[4], Rakesh Lodha[7], Somnath Dutta[3*], Kalpana Luthra[1*]

[1]Department of Biochemistry, All India Institute of Medical Sciences, New Delhi, India
[2]ICGEB-Emory Vaccine Center, International Center for Genetic Engineering and Biotechnology, New Delhi, India
[3]Molecular Biophysics Unit, Indian Institute of Science, Bangalore, India
[4]Department of Biophysics, All India Institute of Medical Sciences, New Delhi, India
[5]Indian Institute of Technology, Roorkee, India
[6] Centralized Core Research Facility, All India Institute of Medical Sciences, New Delhi, India
[7] Department of Pediatrics, All India Institute of Medical Sciences, New Delhi, India

[†]These authors contributed equally
[*]Correspondence**:** kalpanaluthra@gmail.com (K.L.), somnath@iisc.ac.in (S.D.)

**Keywords:** HIV-1 vaccine, Immunogenicity**,** Neutralizing Antibodies, Cryo-EM structure

## ABSTRACT

The envelope (Env) glycoprotein derived from circulating viruses in elite-neutralizers (who naturally develop broadly neutralizing antibodies (bNAbs)), serves as potential template for HIV-1 vaccine design. Herein, we report the structure and immunogenicity of soluble clade-C HIV-1 Env trimer (330) derived from a pediatric elite-neutralizer (AIIMS_330). Using SOSIP, NFL and ferritin-nanoparticle (NP) platforms, we engineered immunogens that preserved native-like Env conformation, exhibited high thermostability and nanomolar affinity for diverse bNAbs, with minimal reactivity to non-neutralizing antibodies. Cryo-EM structure solved at 5 Å resolution of 330-SOSIP trimer-autologous bNAb 44m complex revealed interactions at GDIR motif, N332 supersite along with additional contacts at E293, K337, K446 and glycans N326, N442, N448, as compared to our previously reported BG505–44m structure. Rabbit immunizations with soluble and NP-displayed formats elicited autologous, and heterologous neutralization of tier-1 clade-C

viruses. Herein we define a structurally resolved HIV-1 clade C Env that supports multivalent vaccine strategies and provides mechanistic insights toward rational HIV-1 immunogen design.

## INTRODUCTION

A critical goal in HIV vaccine development is to elicit broadly neutralizing antibodies (bNAbs) in uninfected and high-risk individuals[1]. Elite neutralizers (ENs), a rare group of HIV-1-infected individuals who develop exceptionally potent bNAb responses, provide valuable blueprints for rational HIV-1 immunogen design, aimed at inducing similar bNAb responses upon vaccination[1–3]. Studies involving simian-human immunodeficiency virus (SHIV) challenges in nonhuman primates (NHPs) have indicated that passive immunization with bNAbs can effectively prevent infection, supporting the development of an HIV-1 vaccine that induces such protective immune responses in humans upon vaccination[4–8]. Stabilized HIV-1 envelope (Env) glycoproteins have emerged as promising candidates for immunogen design, with the potential to elicit protective immune responses through vaccination, based on insights from the RV144 Thai trial[9,10]. Native like HIV-1 Env trimers, particularly the clade-A BG505 Env have shown the ability to induce neutralizing antibody (nAb) responses in animal models and are currently under evaluation in clinical trials[11–18]. HIV-1 clade C (HIV-1C), predominates global HIV-1 infection with more than 50% infections[19,20]. A limited number of clade-C Envs has been stabilized; with low expression levels and instability, posing hurdles to develop clade C Env-based vaccines[21–24].

Recent investigations highlight distinct differences in surface antigen presentation between HIV-1 and HPV, contributing to HIV-1's limited ability to elicit a strong immune response compared to HPV[25]. In contrast, currently approved multivalent vaccines for HPV and HBV generate robust immune responses with >95% efficacy[26–28]. Recent studies suggest that single Env-based vaccine regimens may not be the most effective approach for HIV-1 prevention. Notably, presenting HIV-1 Env trimers on self-assembling ferritin nanoparticles has shown promise in eliciting robust immune response in rabbits, suggesting improved immunogenicity[29,30]. Studies also suggest that HIV-infected children who often acquire the infection through vertical transmission, are inherently better at generating bNAbs than adults[31–36]. The relative immaturity of the immune system in children may allow for more effective protective immune responses, as founder virus encounters minimal selection pressure,

63 providing the evolving B-cells an advantage in generating NAbs that effectively neutralize
64 contemporary viruses[31–33,37]. Env trimers from contemporaneous viruses can serve as effective
65 tools for immunogen design, and structural characterization of Env in complex with autologous
66 bNAbs from the same donor can provide valuable insights for vaccine development[36].

67 We previously reported on a pair of HIV-1-infected monozygotic twins (AIIMS_330 and
68 AIIMS_329) demonstrating elite neutralizing activity, with longitudinal sampling of AIIMS_330
69 revealing sustained elite neutralizing activity. The Env from this EN exhibited multiple broad
70 bNAb epitope specificities, making it an ideal template for designing and characterizing HIV-1
71 Env mimics[33,35]. In this study, we designed and characterized an HIV-1 Clade-C 330 Env trimer
72 derived from a pediatric EN AIIMS_330, as soluble SOSIP & NFL Env trimers, alongside tailoring
73 the Env to display a repetitive array of HIV-1 trimers on self-assembling ferritin nanoparticles
74 (NPs)[11,29,38]. Designed Env constructs, stabilized by trimer-stabilizing mutations, exhibited
75 enhanced expression and a greater propensity to assemble into native-like HIV-1 Env
76 mimics[12,15,39,40]. The 330 Env constructs exposed multiple epitopes and demonstrated strong
77 affinity to bNAbs while occluding the immunodominant epitopes of non-neutralizing antibodies
78 (non-NAbs). Ferritin NPs exhibited strong immunogenicity and tier-1 autologous neutralizing
79 activity, upon immunization in rabbits compared to soluble counterparts. Negative stain-
80 electron microscopy (NS-EM) showed that both soluble Envs and multivalent NPs adopted
81 native-like morphology. A cryo-EM structure at 5 Å resolution, revealed a stable, well-organized
82 Envelope structure in the prefusion closed conformation of the 330 SOSIP Env trimer. Structural
83 insights from the cryo-EM model of the 330 SOSIP Env trimer in complex with the autologous
84 bNAb 44m, a V3-glycan-specific potent bNAb identified from the AIIMS_330 EN[36], define the key
85 determinants of autologous bNAb recognition. Collectively, this study provides mechanistic
86 insights into Env–autologous bnAb interactions and expands our understanding of the
87 immunogenicity of HIV-1C Env derived from pediatric elite neutralizers. The 330 Env represents
88 a valuable antigenic probe for HIV-1 bNAb discovery and a potential HIV-1C based Env for a
89 multivalent vaccine design.

90 **RESULTS**

91 **Design & biophysical characterization of 330 Env trimers and ferritin nanoparticles**

92 Previously we reported a pair of HIV-1 chronically infected monozygotic twins AIIMS_330
93 & AIIMS_329 exhibiting elite plasma neutralizing activity[35]. Over five years of longitudinal
94 sampling, the AIIMS_330 EN showed sustained evolution of plasma bNAbs targeting major
95 neutralizing determinants on the HIV-1 Env glycoprotein[33,35,41]. The pseudoviral Env clone
96 330.16.E6, derived from the AIIMS_330 EN, exhibited high susceptibility to neutralization by a
97 broad range of HIV-1 bNAbs with multiple epitope specificity, along with autologous
98 contemporaneous plasma antibodies, and resistance to the panel of non-nAbs tested[33,35].
99 Therefore, we engineered this Env in membrane soluble forms, as SOSIP.664 gp120-gp41
100 cleaved Env trimers, NFL.664 gp140 single-chain uncleaved Env trimers and SOSIP Env trimers
101 on self-assembling ferritin NPs to achieve multivalency (Figure 1 A-C). The 330 Env trimers were
102 stabilized by incorporating mutations for increased expression and trimerization, as illustrated
103 in Figure 1A-D, Table S1. The SOSIP Env was designed by introducing a SOS disulfide bond
104 (A501C-T605C)[42], an I559P mutation[43], and an optimized furin cleavage site (RRRRRR)[44] . We
105 designed the NFL Env construct, that carried the I559P mutation, by linking the gp120 and gp41
106 using a flexible glycine-serine linker (GGGGSGGGGS)[38]. Both Env constructs were human codon-
107 optimized to enhance expression in mammalian systems.

108 The stabilized and optimized 330 Envs were expressed in HEK293F cells, followed by a
109 two-step purification viz. HIV-1 Env trimer specific bNAb PGT145-Immunoaffinity
110 chromatography followed by Size Exclusion Chromatography (SEC). The SEC purification of 330
111 Env trimers (SOSIP and NFL) yielded a peak at an elution volume of 10 mL, which shifted further
112 upward for ferritin nanoparticles, eluting at 8.5 mL on a Superdex 200 10/300 column (Figure
113 1E). The purification yield of 330 Env trimers following SEC was around ~1 mg/L for SOSIP and
114 ~1.45 mg/L for NFL (Figure S2), which was higher or comparable to the Indian and South
115 African Clade-C strains (CZA97: ~0.4-0.6 mg/mL, 329 SOSIP: ~0.6 mg/mL, 16055 NFL: ~2
116 mg/mL)[23, 45–47]. The NFL trimer of Env 330 had better expression yields than the SOSIP version,
117 likely due to the increased stability and functionality provided by the covalent linkage between
118 the gp120 and gp41 subunits, resulting in more functional gp140 molecules[38,47]. However, low
119 yield of Ferritin NPs was observed, around 0.05 mg/L, likely due to the complex assembly of Env
120 trimers into synthesized ferritin nanocages as reported previously[48,49]. The 330 Env trimers
121 displayed single band on Blue Native-PAGE (BN-PAGE) stained with Coomassie, whereas the 330
122 ferritin NPs were too large to efficiently enter the gels and visible at the top of the lanes,

123 indicating the high purity of Env trimers and NPs preparations (Figure S2-Left). The SDS-PAGE
124 analysis revealed intact trimeric nature of the 330 Env proteins under non-reducing conditions
125 that separated as monomers in the presence of DTT under reducing conditions (Figure S2-
126 Right). Negative-Stain Electron Microscopy (NS-EM) reference-free two-dimensional (2D) class
127 averages demonstrated that over 99% of the gp140 proteins adopted a native-like trimeric
128 morphology, with multiple copies of the Env spikes efficiently displayed on the self-assembling
129 ferritin NPs (Figure 1F, Supplementary S3). The 3D reconstruction of soluble gp140 trimers
130 reveals a trilobular structure and while predicted model of ferritin NPs display multiple copies of
131 Env spikes (Figure 1G). Thermal stability & secondary structures of 330 Envs were evaluated
132 using sypro-orange Differential Scanning Fluorimetry (DSF) and by Circular Dichroism (CD)
133 spectroscopy. The 330 SOSIP Env exhibited a Tm of ~74°C indicating its ability to retain its
134 structural integrity even at elevated temperatures (Figure 1H, S4 A-B). The CD spectra of 330
135 SOSIP Env reveal ~25% alpha-helical and ~25% antiparallel beta-sheet content, contributing to
136 the stability and rigidity of the Env, while random coils impart the flexibility required for
137 molecular recognition, collectively suggesting a thermodynamically stable secondary structure
138 for the Envelope protein (Figure S4 C-D). Overall, biophysical characterization demonstrated
139 that the 330 Envs are well-stabilized, and effectively displayed on ferritin NP cages.

140 **Antigenicity of 330 Env trimers and ferritin nanoparticles indicated strong binding**
141 **affinity to HIV-1 bNAbs**

142 Next, we assessed the antigenicity of the 330 Envs using binding ELISA with an extensive
143 panel of HIV-1 bNAbs and non-nAbs. The 330 Env trimers exhibited well-exposed epitopes
144 recognized by potent bNAbs, including the V1V2 apex (PGT145, PGDM1400, CAP256.25), the V3-
145 glycan supersite (2G12, PGT121, 10-1074, AIIMS-P01), the CD4 binding site (VRC01, N6), and
146 the gp120-gp41 interface (PGT151), while showing minimal reactivity to non-NAbs (F105, A32,
147 48d, 17b+sCD4), suggesting that the 330 Env trimers adopt native-like conformations (Figure 2).
148 The antigenic profile of ferritin NPs was found to resemble that of SOSIP, though with less
149 saturation at the tested monoclonal antibodies(mAbs) concentration and allowing all the
150 conformational epitopes to be accessible to HIV-1 neutralizing mAbs targeting to the Envs
151 presented on the nanoparticle. A minor degree of binding of the non-NAbs was observed with
152 NFL and ferritin particles, with negligible binding to SOSIP. Notably, the 330 Env trimers and
153 particles exhibited preferential affinity for neutralizing mAbs over non-neutralizing mAbs.

154 Subsequently, we assessed the binding affinity of 330 Envs to neutralizing & non-
155 neutralizing mAbs with distinct specificities by BLI-Octet analysis. To assess binding affinity and
156 kinetics, we selected conformation-specific bNAbs (PGT145, PGDM1400, and PGT151) as well as
157 non-neutralizing antibodies (F105, 17b, and sCD4). The gp140 Envs (affinity) & ferritin NPs
158 (avidity) exhibited strong binding affinity to the tested bNAbs (Figure 3). The SOSIP variants
159 (Ferritin NPs) (KD 1.07 nm) & NFL (KD 1.39 nm) showed a high affinity of ~1nM to the V1V2
160 directed bNAb PGT145. A similar trend in binding of PGDM1400 with SOSIP (KD 1.34 nm) & NFL
161 Env (KD 3.32 nm) was observed respectively. The interface-directed bNAb PGT151
162 demonstrated an exceptionally high affinity to SOSIP variants (Ferritin NPs), with an affinity of
163 ~5 pM, indicating that the PGT151 epitopes on the Env proteins displayed on the nanoparticle
164 were highly accessible (Table S2). We observed that PGT145-purified SOSIP trimers were
165 efficiently cleaved at the gp120-gp41 junction, as indicated by strong binding to the cleavage-
166 specific bNAb PGT151, while no binding was detected with NFL trimer (Figure 2 & 3). The
167 introduction of intraprotomer locking 201C –433C disulfide bond as described previously[47], in
168 these constructs prevented the CD4-induced Env rearrangements as assessed by low reactivity
169 with sCD4 & 17b non-nAbs, indicating the prefusion conformation of the Envelopes. As expected,
170 and consistent with the ELISA binding results, the 330 Envs exhibited minimal reactivity to the
171 non-NAbs F105 and 17b+sCD4 (Figure 2 & 3, Table S2). Collectively, these findings suggest that
172 both the soluble Envs and multivalent NPs adopt a native-like conformation, exposing multiple
173 key bNAb epitopes while shielding the immunodominant epitopes targeted by non-NAbs. Based
174 on the negligible antigenic reactivity of the SOSIP Env with non-nAbs, we next performed the
175 structural analysis of the SOSIP Env.

176 **Cryo-EM structure of 330 SOSIP Env in complex with autologous bNAb 44m**

177 The structure of the natively glycosylated 330 SOSIP Env was solved using single-particle
178 cryo-electron microscopy (cryo-EM). A total of 109004 particles were analyzed to determine the
179 2D class averages and reconstruct the trilobular 3D model of 330 SOSIP Env in its prefusion
180 closed conformations (Figure S5 A-C). In a recent study, we reported heavy chain matured HIV-1
181 lineage bNAb 44m, which effectively neutralizes its autologous pseudovirus, 330.16.E6, from
182 which the 330 Env trimer is derived[36]. The cryo EM structure was solved at 5 Å, to map the key
183 interacting epitopes on the clade C Env 330 with its autologous bnAb 44m. The architecture of
184 330 Env displayed the trilobular shapes of trimers with three extra densities of corresponding

185 bNAb 44m Fab bound moieties (Figure 5 A-B, Supply S6). The model showed that three 44m
186 Fab's bind to each gp120 monomeric subunit, enabling effective neutralization (Figure 5C-D).
187 The interacting surface area covered by the mainly by heavy chain of 44m and 330 Env are 690
188 $Å^2$, and 613 $Å^2$ respectively (Figure 5C-D). The model further reveals that the 44m CDRH1 is
189 positioned near the 330 Env V1V2 loop, while CDRH2 and CDRH3 are located near the V3 region
190 (Figure 5E). The 330-SOSIP trimer- 44m bNAb complex revealed interactions at the GDIR motif,
191 N332 supersite along with additional contacts at E293, K337, K446 and glycans N326, N442,
192 N448, as compared to our previously reported BG505–44m structure[36]. Within the GDIR motif of
193 the 330 env, we found interactions of 44m with the R327 in addition to the D325 residue, while
194 earlier solved cryo EM structure of the BG505-44m complex showed D325 dependence alone.
195 The distinct key interacting residues identified in case of autologous Env 330 as compared to the
196 heterologous clade-A Env BG505 include S30 in the CDRH1 loop, which forms a contact site with
197 R327 in the V3 loop; Y52 and Y53 in the CDRH2 loop, which interact with R327, and H330 in the
198 V3 region; R109 in the CDRH3 loop, which engages with E293 of C2 region, and K337 in the C3
199 region; and K446 in the C4 of gp120; R78 residues from FR3 loop interacts with D325 in the V3
200 region (Figure 5E-F). Therefore, both CDRH2 and FR3 loops interact with the GDIR motif in the
201 V3 region of envelope. These interactions are primarily stabilized through electrostatic
202 interactions, hydrogen bonding, and van der Waals forces. Epitope mapping of the 44m bNAb on
203 its autologous Env revealed that the antibody engaged a peptide surface area of 1305.3 $Å^2$ and a
204 glycan surface area of 788.65 $Å^2$ on gp120 (Figure S7). The electrostatic surface potential map of
205 44m showed the facing of E293, D325, R327, H330, N332, K337, and K446 residues towards the
206 charged and hydrophilic regions of the 44m bnAb (Figure 5G). The glycan interaction at the 330
207 Env-44m Fab junction involves N301 and N332 from the V3 loop, and N397 in V4 loop, N442,
208 and N448 from the C4 region (Figure 5H). Next, we performed structural superimposition of the
209 44m-BG505 atomic model into our atomic model (Figure S8). This analysis allowed us to
210 investigate the binding modes of 44m[36] and other V3-glycan specific bNAbs 10-1074[50],
211 PGT121[51], 438-B11[52], BG18[53], mature BG18[54], DH270.6[55], and BF520.1[56] to a 330 Env
212 superimposed BG505 model. Our findings suggest that 44m interacts with the V3 loop via a
213 slightly declining shift, similar to BF520 and BG18, but exhibits a distinct binding mode
214 compared to PGT121 and 35O22 (Figure S8).

215 **Structural and glycan homology of 330 Env to BG505**

216 To assess structural similarity, The HIV-1 Clade C 330 SOSIP trimer was superimposed
217 onto a clade C Env 16055 NFL[57] (PDB: 5UM8) and a Clade-A Env BG505 SOSIP[58] (PDB: 4TVP). We
218 observed that the 330 Env trimer exhibited greater structural similarity to BG505 Env, with
219 lower root-mean-square deviations (RMSDs) of 0.685 Å for gp120 and 0.478 Å for gp41
220 compared to modelled 16055 Env, which had RMSDs of 0.798 Å for gp120 and 0.739 Å for gp41
221 (Figure 4A-D). Upon glycan prediction analysis by Los Alamos HIV-1 sequence database
222 (LANGT), we observed that 330 Env lacked conserved PNGS at positions 295 and 339 in the
223 V3/C4 region and at position 130 in the V1V2 apex, in contrast to BG505 Env, which lacks PNGS
224 at positions 241 and 289 (Figure 4E). Next, we calculated the total glycan hole area in the 330
225 Env using Los Alamos glycan shield mapping tool (LAGSM), suggesting that the optimal protein
226 accessible area was 967 $Å^2$, compared to BG505, B41, C9Z7A & Du422 counterparts (Figure 4F).
227 The potential N-glycosylation sites (PNGS) conserved in the 330 Env were determined by Los
228 Alamos HIV-1 sequence database (LANGT) using N-Glycosite tool. Conserved PNGS analysis
229 revealed that 330 Env comprises of 28 PNGS comparable to that reported in the BG505[59]&
230 16055[60] Envs (Figure 4F, Table S3). Targeting exposed protein surfaces within glycan holes can
231 be an effective strategy to boost the immune response against these vulnerable sites. Overall, our
232 structural homology modelling and glycan analysis demonstrate that the stabilized clade-C Env
233 330 shares numerous features with the well-studied BG505 Env and suggesting its capacity to
234 adopt well-ordered structures.

235 **330 Ferritin nanoparticles and SOSIP trimer exhibit enhanced immunogenicity compared**
236 **to NFL in rabbits**

237 Following the establishment of native-like prefusion-closed Env structures, we further
238 evaluated and compared the immunogenicity of soluble Env trimers (SOSIP & NFL) and
239 multivalent ferritin NPs in New Zealand White (NZW) rabbits. Four groups of female rabbits
240 were immunized, primed at week 0, and boosted at weeks 4 and 20 and administered a dose of
241 20 μg of 330 gp140 Env trimers or an equimolar amount (25 μg) of ferritin nanoparticles,
242 formulated with AddaVax™ adjuvant (Figure 6A). The AddaVax™ adjuvant is a squalene-based
243 oil-in-water nano-emulsion and has been shown not to impact the structural integrity or
244 antigenicity of the Env trimers, as demonstrated in previous studies[61,62]. Rabbits were bled at
245 weeks 0, 4, 6, 16, 20, and 22 and sera samples were subsequently evaluated for binding
246 reactivity with the Env trimer using capture ELISA and for neutralizing activity against Env

247 pseudotyped viruses. First, we evaluated the binding titers of the collected immune sera from
248 different timepoints against the immunogens tested and measured as median titers across each
249 group. The binding titers of immune sera exhibited a significant increase between 4 to 8 weeks
250 and then again between 20 to 22 weeks, immediately after the second and third boosters (Figure
251 6B). The polyclonal immune sera demonstrated sustained binding reactivity to the autologous
252 Envelope trimer and with the cross-clade Envelopes, though with a lower extent to heterologous
253 Envs. The half-lives ($t1/2$) of the immune sera titers against the autologous Env were
254 significantly longer (p value: 0.007) as compared to that of the heterologous Envs (SF162, 6240,
255 1086) tested. The overall immune sera binding titers were comparable across the test groups;
256 however, rabbits immunized with 330 SOSIP and ferritin NPs exhibited statistically significantly
257 antibody titers (p value: 0.01) compared to those immunized with NFL counterparts. Peak serum
258 antibody binding to 330 Env was observed at week 22, prompting further analysis of week 22
259 serum samples for their neutralization activity.

260 Neutralization breadth was further evaluated against autologous (330.16.E6), closely
261 related (329.14.B1), and heterologous clade C (MW965.26 and 25925), Tier 1 clade B (SF162),
262 and Tier 2 clade A (BG505.T332N) pseudoviruses. No immune sera response was detected
263 against murine leukemia virus (MLV) used as a negative control and all animals exhibited
264 neutralizing antibody responses following immunization, except for one in the NFL group
265 (NZW5273) (Table S4). Multivalent 330 ferritin NPs and SOSIP elicited a strong neutralizing
266 response against autologous (330.16.E6) and closely related Envs (329.14.B1) as compared to
267 NFL counterpart. The Ferritin NP group elicited the most robust autologous neutralizing
268 antibody response, with a median $ID_{50}$ titer of 1160 compared to the soluble gp140 trimer
269 groups (SOSIP and NFL) with median $ID_{50}$ titers of 830 and 375, respectively (Figure 6C). The
270 Ferritin NP group demonstrated a statistically significant increase in neutralizing antibody titers
271 compared to both the SOSIP ($p = 0.014691$) and NFL ($p = 0.010323$) groups, with fold
272 differences of 2.5-fold and 3.5-fold, respectively. These findings were consistent with the results
273 from the capture ELISA, where the NP and SOSIP groups exhibited sustained binding reactivity,
274 whereas the NFL group showed a decline in response after boosters. The NP and SOSIP groups
275 demonstrated moderate heterologous neutralizing responses against the clade C Tier 1 viruses
276 (MW965.26 and 25925) and the Tier 1 clade B virus (SF162), with responses comparable to each
277 other and higher than the NFL group although the differences were not statistically significant.

None of the 330 immunogens induced neutralizing responses against the Tier 2 BG505 virus, which aligns with the low BG505 nAb activity observed in the plasma of the AIIMS_330 HIV-1-infected elite neutralizer[35]. Overall, we observed that both 330 SOSIP Env trimer and ferritin NPs elicited strong autologous NAb responses, as well as cross-clade neutralization, though with a limited magnitude. Notably, the presentation of these antigens on ferritin NPs were associated with a higher trend in NAb response induction.

## DISCUSSION

HIV-1 clade-C accounts for more than half of global HIV-1 infections, with particularly high prevalence in South Africa and India[19,20]. Comparative analyses of clade-C viruses from these regions reveal the significant differences in their sequences, highlighting distinct evolutionary trajectories[63]. These regional variations in intra-clade-C Env sequences likely contribute to the differential sensitivity of circulating strains to HIV-1 nAbs. HIV-1 Clade-C characterized by unique features such as enhanced transmission efficiency, extensive genetic diversity within the V1-V3 region of the Env gene, and a distinct profile of drug resistance mutations compared to other clades[63–66]. Understanding these differences is crucial for tailoring the prevention and treatment strategies in clade C prevalent regions[19,20]. Structural information on the HIV-1 Env trimer from clade-C is crucial for structure-guided immunogen design. However, only a limited number of high-resolution structures are available for native-like clade-C Env trimers, such as 16055[47,67], DU172.17[68], 426c[69], and CZA97.12[70]. Although many HIV-1 Env immunogens have been stabilized, most studies have extensively characterized BG505, a Clade-A transmitted founder Env derived from a 6-week-old infant with elite neutralizing activity[11]. Such elite individuals from the pediatric group could provide valuable Env immunogen templates, as HIV-1 infection and disease progression in children differs from that in adults[31,34,35]. Notably, neutralizing antibodies tend to arise early in the course of infection in pediatric individuals, with the ability to neutralize contemporaneous viral Envelopes[33,37]. We previously reported a pair of monozygotic twins (AIIMS_329 and AIIMS_330) with elite neutralizing activity, whose plasma demonstrated exceptionally potent bNAb responses with multi-epitope specificities against a diverse panel of multi-clade heterologous Env pseudoviruses[33,35]. These Envs hold significant potential as templates for vaccine design and as antigenic baits to isolate HIV-1 bNAbs for immunotherapeutic applications[46]. Recent studies demonstrated that, multimeric presentation of viral class I fusion viral glycoproteins, such as , Ebola virus Glycoprotein (GP)[71,72], influenza

309 hemagglutinin (HA)[73,74], Respiratory Syncytial Virus (RSV) F protein[75,76], SARS-CoV-2 S
310 protein[77–80] and HIV-1 Env[29, 30] on ferritin NPs have enabled efficient production of well-ordered
311 NP-based vaccine candidates with a capacity to induce robust immune response.

312 Here we report a soluble HIV-1C 330 native-like Env trimer on SOSIP and NFL platform,
313 derived from a circulating virus in an Indian pediatric EN AIIMS_330[35], by stabilizing the Env
314 using version 7 mutations and displaying the SOSIP Env on self-assembling ferritin NPs[29,30]. The
315 purification yield of Env trimers post SEC was around ~1 mg/L for SOSIP and ~1.45 mg/L for
316 NFL, which was higher or comparable to the Indian and South African Clade-C strains (CZA97:
317 ~0.4-0.6 mg/mL, 329 SOSIP: ~0.6 mg/mL, 16055 NFL: ~2 mg/mL, 1PGE-THIVC SOSIP)[23,45–47].
318 Using Negative stain Electron Microscopy, we demonstrated that SOSIP and NFL Envs displaying
319 key features of native-like trimeric conformation and Env trimers were presented efficiently on
320 ferritin NPs as observed in stabilized BG505 Env-particles[29]. The structure of the 330 SOSIP,
321 resolved by single-particle cryo-EM, revealed trilobular Env structures in their prefusion, closed
322 conformation. The generated Env trimer and particles displays a desirable antigenic profile, with
323 nanomolar affinity to conformation specific bNAbs (PGT145 & PGT151), with negligible
324 reactivity to non-nAbs (F105 & 17b+sCD4), shielding the Env immunodominant regions.
325 Biophysical characterization showed that the 330 Env exhibits a balanced thermodynamic
326 profile and high degree of thermal stability with a Tm of ~74°C which is notably higher as
327 compared to other reported clade C Envs ZM197 (69°C)[12] , IPGE-THIVC (62°C)[23] and 16055
328 (68°C)[81]. We observed greater structural similarity of 330 Env to clade-A BG505 Env (RMSD
329 gp120-0.685 Å & gp41-0.478 Å) compared to clade-B AMC009 Env reported (RMSD gp120-2.623
330 Å & gp41-1.624 Å), suggesting well-ordered structures[14].

331 Cryo-EM structure of 330 Env in complex with autologous bNAb 44m at 5 Å resolution
332 revealed the well-exposed epitopes; the three trilobular structures occupied by the three Fab
333 arms. We identified herein, additional key antigenic determinants E293, K337, K446 in the
334 autologous 330 Env, that interacted with 44m; in addition to D325, R327 and N332 dependency,
335 as observed with heterologous BG505 Env[36]. Further, the additional interaction within the GDIR
336 motif, of the R327 along with the D325 residue as observed in the solved structure of 330 with
337 44m, plausibly contributed to the potent neutralization of the autologous virus 330.16.E6. Our
338 findings offer crucial insights into the antigenic determinants in the clade C virus Env, that
339 interact with the autologous antibody 44m, that can inform a clade-based vaccine design.

340 Furthermore, using a reverse vaccinology approach, these insights can guide the structure-based
341 engineering of neutralizing antibodies[82].

342 Rabbit immunizations demonstrated that the 330 Env immunogens elicited robust
343 immune responses against autologous and other tier-1 viruses tested, with limited cross-clade
344 neutralization. This may be attributed to distinct antigenic determinants on heterologous Envs,
345 adjuvant used or by varied glycan compositions[83,84]. Further insight can be achieved by
346 investigating the specific epitopes targeted by NAbs in the immune sera, however it has not been
347 addressed herein and is a limitation of this study. The multivalent presentation of HIV-1 antigens
348 on ferritin NPs correlated with enhanced neutralization potency, likely attributed to augmented
349 B-cell activation signals[85]. This observation aligns with findings from germline-targeting eOD-
350 GT8 NPs, suggesting a potential mechanism for eliciting more robust and coordinated immune
351 responses[85]. These findings emphasize the need for further exploration of the role of glycans and
352 structure guided mutations in shaping immunogenicity.

353 In summary, we designed and characterized soluble HIV-1C Env trimers derived from a
354 pediatric elite-neutralizer from India. Structural analysis of the 330 Env trimer in complex with
355 autologous bNAb 44m, a heavy chain matured version of the first bNAb AIIMS_PO1, identified
356 from the AIIMS_330 donor, revealed molecular features of 330 Env-44m bNAb interaction which
357 could inform structure-based vaccine design. Our findings indicate that the HIV-1C 330 SOSIP
358 Env trimer can serve as a valuable antigenic probe for bNAb discovery and is a promising
359 candidate for multivalent HIV-1 vaccine design and development.

360 **MATERIALS AND METHODS**

361 **Institutional Review Board & Ethics approval**

362 This study was conducted after obtaining approval from the institutional ethics committee, All
363 India Institute of Medical Sciences (AIIMS), New Delhi, India (250/IAEC-1/2020). Rabbit
364 immunization was outsourced to a contract research organization (CRO) Liveon Biolabs Private
365 Limited, Bengaluru, Karnataka, India with IAEC (IAEC-approved protocol No.: LBPL-IAEC-008-
366 01/2021; study number: LBPL/NG-1736 (EF)). The immunization studies described here were
367 carried out on female naive New Zealand White rabbits of 2.0–2.5 kg and aged 4 months. All
368 animal experiments adhered to the guidelines for the care and use of laboratory animals as

369 outlined by the Committee for Control and Supervision of Experiments on Animals (CCSEA),
370 Government of India[86].

371 **Construct design**

372 The 330 Env gene was derived from a previously identified Indian clade C HIV-1 Env (330.16.E6,
373 GenBank: MK076720) obtained from a pediatric elite-neutralizer AIIMS_330, as previously
374 described[35]. The 330 Env construct were design in soluble forms as SOSIP.664[11] gp120-gp41
375 cleaved Env trimers and NFL.664[38] gp140 single-chain Env trimers along with tailoring of SOSIP
376 Env trimers on self-assembling ferritin nanoparticles[29] to achieve multivalency. SOSIP & NFL
377 constructs were stabilize by incorporating I559P & ΔMPER (Env prefusion stabilizing
378 mutation)[43,87], R315Q (reduced V3 non-nAb immunodominant exposure)[88], I201C-A433C
379 (intraprotomer locking disulfide bond, reduced V3 exposure)[12], and clade C stabilizing B505-
380 Trimer Derived (TD8) mutations (E47D, T49E, V65K, I165L, K429R, K432Q, K500R)[39]. The SOSIP
381 construct was designed by introducing an SOS disulfide bond (A501C-T605C)[42], an I559P
382 mutation[43], and an optimized furin cleavage site (RRRRRR)[44]. In contrast, the NFL (Native
383 Flexible Linker) construct retained the I559P mutation and linked gp120 and gp41 using a
384 flexible glycine-serine linker (GGGGSGGGGS)[38]. Native signal sequence is replaced by the CD5
385 signal peptide (MGSLQPLATLYLLGMLVASVLA) for enhanced secretion of Envelope proteins,
386 constructs were codon optimized for mammalian expression and synthesized commercially by
387 GeneArt (Thermo Fischer Scientific). For binding assays, 330 Env constructs were tagged with
388 either a His-tag (GSGSGGSGHHHHHHHH) or a twin strep tag (tst)
389 (WSHPQFEKGGGSGGGSWSHPQFEK) at the C-terminus of gp41ECTO, preceding the stop codon.
390 These constructs were subsequently cloned into pPI4 expression vector using Pst1 and Not1
391 restriction sites. The 330 ferritin NP's construct was generated by fusing the N-terminus from
392 *Helicobacter pylori* ferritin (GenBank: WP_000949190.1), starting from Asp5 to Ser167, to the
393 SOSIP.664 C-terminus (truncated at position 664), separated by a Gly-Ser (GSG) linker, as
394 described previously[29].

395 **Envelope Protein Expression**

396 The 330 Env encoding plasmids were transiently expressed in 293F suspension cells (Gibco,
397 R790-07). 293F cells were thawed and maintained in Freestyle Expression Medium (Gibco,
398 K9000-01) in a Shaker incubator at 37°C, with 120 r.p.m. and 8% CO2. For transfection, HIV-1

399 Env and furin protease encoding plasmids mixed in a 3:1 ratio (w/w) with NFL (500 μg), SOSIP
400 Env (333.3 μg), to furin (166.6 μg) incubated with transfection reagent PEImax (Polysciences,
401 24765) in a 3:1 ratio (w/ w) PEI max to DNA for 20 min at room temperature (RT) and then
402 added to 1L culture at density of 1 million cells/mL. Seven days post-transfection, the
403 supernatants were harvested, centrifuged, and filtered using 0.45-mm filters (Nalgene,
404 2954545).

405 **Envelope Protein Purification**

406 330 SOSIP Env and SOSIP Env-NP fusion proteins were purified by PGT145 bNAb
407 immunoaffinity chromatography, as described previously[45]. Briefly, HIV-1 pre-fusion closed
408 trimer-specific bNAb PGT145[89] was covalently coupled to the CNBr-activated Sepharose 4B
409 beads (GE Healthcare, 17043001) according to the manufacturer's protocol for antibody
410 coupling. The PGT145-coupled CNBr Sepharose 4B bead column was used to purify HIV-1 Env
411 trimers or Env trimer NPs. Env proteins contained in Expi293F filtered supernatants were
412 captured on PGT145-coupled CNBr-activated sepharose beads by overnight rolling incubation at
413 4 °C. Subsequently, the mixture of supernatants and beads was passed over Econo-columns
414 (Biorad, 7371512). The columns were then washed with three column volumes of 0.5 M NaCl
415 and 20 mM Tris HCl pH 8.0 solution. After elution with 3 M $MgCl_2$ pH 7.5, the proteins were
416 buffer-exchanged into TN75 (75 mM NaCl, 20 mM Tris HCl pH 8.0) or PBS buffer by
417 ultrafiltration with Vivaspin concentrators MWCO 100 kDa (Cytivia, 28932363). Protein
418 concentrations were determined from the A280 values measured using a NanoDrop One
419 (Thermo Fisher Scientific, 29018226) and the molecular weight and extinction coefficient values
420 were calculated by the ProtParam Expasy webtool. Env proteins used for immunization were
421 first purified using PGT145 affinity chromatography, followed by size-exclusion chromatography
422 (SEC) on a Superdex 200 Increase 10/300 GL column (28990944, GE Healthcare Life Sciences)
423 using an Äkta Pure 25M system (Cytiva, 29018226). Envs containing fractions were pooled,
424 concentrated, filter-sterilized, snap-frozen in liquid nitrogen, and stored at -80°C until further
425 use.

426 **SDS-PAGE and BN-PAGE Analyses**

427 For SDS-PAGE and blue native polyacrylamide gel electrophoresis (BN-PAGE) analyses, 2 μg of
428 330 gp140 Env trimers, or equimolar amounts of ferritin NP's (2.5 μg) was ran over precast

429 native gel 4–20 % Bis-Tris gradient gel (Biorad, 4561094). The degree gp120-gp41 cleavage was
430 examined by incubating the SOSIP & NFL protein with 0.1M dithiothreitol (DTT) and analysed by
431 SDS-PAGE under reducing conditions. Subsequently, gels were stained with the Colloidal Blue
432 Staining Kit (Invitrogen, LC6025), respectively.

433 **Enzyme linked Immunosorbent assay (ELISA)**

434 ELISAs were performed as previously described[90] using tst-tagged Env constructs on
435 StrepTactinXT-coated microplates (IBA Lifesciences, 2-4101-001). Purified proteins (1 µg/mL)
436 were diluted in NaHCO3 buffer and immobilized on 96-well Streptactin plates by O/N incubation
437 at 4°C. Following a three wash step with PBST (0.05% Tween20) to remove unbound trimers,
438 plates were blocked by 1% BSA in PBST for 2 hours at RT. Further the serial dilutions of test
439 antibodies ranging from 10ug – 0.004 ug/ml in PBST/1% BSA solution were added and
440 incubated for 2 h. After 3 washes with PBST, HRP-labelled goat anti-human IgG (Jackson
441 ImmunoResearch, AB_2337578) diluted 1:3000 in PBST/1% BSA was added and incubated for
442 30 mins, followed by 3 washes with PBST and 3 washes of PBS. A developing solution (1% TMB
443 (Mabtech, 3652-F10), allowed the colorimetric reaction, which was stopped by the addition of 2
444 N H2SO4. Finally, colour development (absorption at 450 nm, OD450) was measured at
445 NanoDrop One (Thermo Fisher Scientific, 29018226) to obtain the different binding curves.

446 **Biolayer Interferometry (BLI)**

447 Binding kinetics were measured using an Octet K2 (ForteBio, RED96e) device at RT with 1000
448 rpm agitation. Anti-human Fc sensors (Sartorius AHC, 18-5060) were used to capture mAbs on
449 the Octet K2, were equilibrated in kinetics buffer for 60 s to obtain a baseline prior to protein
450 association. 330 Envelope protein was used as analyte in concentrations ranging from 210 to 2.6
451 nM in the HEPES buffer (pH 7.2) background supplemented with 0.02% Tween 20 and 0.1%
452 BSA. Binding was assessed by incubating mAb-captured sensors in wells containing 10 µg/ml
453 Env for 120 seconds with 1000 rpm agitation. Association was recorded for 150 s followed by
454 dissociation for 450 s. Data were analysed using the ForteBio Data analysis software (Forte- Bio
455 Inc, Version 9.0) and a global fit was performed using a 1:1 binding model to fit the association
456 and dissociation curves.

457 **Sypro orange differential scanning fluorimetry (DSF)**

458 330 SOSIP protein were prepared at a concentration of 0.2 mg/mL in 1XPBS and transferred into
459 0.1 mL polypropylene PCR tube strips (Tarsons, 611020) with a final volume of 25 µL. Sypro
460 Orange protein stain (Invitrogen, 4461146) was added at a 1:200 dilution. The samples were
461 analyzed using a Rotor-Gene Q system (Qiagen, 9001862) with a high-resolution melt (HRM)
462 protocol, starting at 25°C and increasing to 90°C in 1°C increments, with each step lasting 4
463 seconds. Melt curve data were processed using Rotor-Gene Q Series Software.

464 **Circular dichroism (CD) spectroscopy**

465 The Far-UV spectrum was recorded in the wavelength range of 200–250 nm using a CD
466 Spectrophotometer (JASCO, J-1500) with a 0.1 cm path length Quartz cuvette (Sigma Aldrich,
467 I0285). Measurements were conducted for the 330 protein in a 20 mM phosphate buffer (pH 7.5)
468 with100 mM NaCl concentration at 4˚C for 30 minutes. Each spectral scan was averaged over 2–3
469 measurements. The CD spectra were visualized using SigmaPlot 10.0, and the secondary
470 structure was analyzed through the BESTSEL online server. For thermal studies, measurements
471 were performed between 20˚C and 80˚C using the same Quartz cuvette, and the melting curve
472 was generated using SigmaPlot 10.0.

473 **Negative Stain Microscopy (NS-EM)**

474 Negative-stain electron microscopy (NS-EM) was performed essentially as described
475 elsewhere[91]. Briefly, 3 µl of purified 330 gp140 Env trimers or ferritin NPs (~0.03 mg/mL) were
476 applied to glow discharged (20 mA for 30 s) carbon-coated 400 Cu mesh grid. After 5 s, grids
477 were negatively stained with 2% (w/v) uranyl formate for 60 s. Imaging was performed using a
478 120 kV Talos L120C electron microscope (TALOSL120CMS) equipped with a 4k x 4k Ceta camera
479 at a magnification of 73kx (3.84 Å/pixel). The collected images were processed in EMAN 2.1[92].
480 Particle extraction and reference-free 2D class averages were generated using simple_prime2D
481 in SIMPLE 2.1 software[93] with a mask diameter of 30 pixels at 3.84 Å/pix.

482 **Preparation of 44m Fab fragment**

483 Fab fragments were generated from 4 mg of AIIMS-44m IgG using a Fab fragmentation kit (G
484 Biosciences, 786-273) following the manufacturer's protocol. Briefly, 0.5 ml of 44m IgG was

485 desalted using a SpinOUT™ GT-600 column. Cysteine.HCl was added to the Fab Digestion Buffer
486 (pH) to a final concentration of 20 mM before papain digestion. The 0.5 ml IgG sample was then
487 incubated with Immobilized Papain in the spin column at 37°C for 6 hours with end-over-end
488 mixing. After incubation, the digested antibody solution was collected by centrifugation at 5,000
489 x g for 1 minute. The flow-through was further incubated with Protein A resin for 10-15 minutes
490 at room temperature (RT) with end-over-end mixing. Subsequently, the Fab fragments were
491 collected in the flow-through while Fc fragments and undigested IgG remained bound to the
492 resin. The purity and size of the Fab fragments were assessed by SDS-PAGE and the purified Fab
493 fragments were stored at -80°C.

494 **Cryo-EM sample preparation, data acquisition, data analysis and model fitting**

495 330 Env trimer (1.5 mg/ml) incubated with 44m Fab at 1:3 molar ratio. 3 µl of sample were
496 applied to glow discharged R1.2/R1.3 300 mesh copper grids and immediately blotted for 6 secs
497 with 5 seconds of blotting force using FEI Vitrobot Mark IV plunger at 22°C and 100% humidity.
498 The grid was immediately plunge-frozen into liquid ethane at liquid nitrogen temperature. Cryo-
499 EM data were collected using 200 kV Talos Arctica transmission electron microscope (Thermo
500 Scientific, TALOSARCTICA) equipped with Gatan K2 Summit Direct Electron Detector. Movies
501 were recorded automatically using Latitude-S (DigitalMicrograph - GMS 3.5) at a nominal
502 magnification of 45,000x at the effective pixel size of 1.17 Å[93]. Micrographs were acquired in
503 counting mode with a total dose of 40 $e^-/Å^2$, with an exposure time of 8 sec distributed for 20
504 frames. A total of 6046 movies were acquired for the 330 SOSIP Env trimer and 44m Fab
505 complexes, respectively. Single-Particle Analysis (SPA) was performed for the acquired Cryo-EM
506 movies using the cryoSPARC 4.5 [94]. At first, drift and gain corrections of the individual movies
507 were performed with Patch Motion Correction and estimated Contrast transfer function (CTF)
508 parameters using Patch Ctf estimation. Subsequently, CTF-estimated micrographs were subjected
509 to analysis to eliminate poor-resolution micrographs with a fit resolution threshold of 8 Å using
510 curate exposure. The particles from the best micrographs were chosen for automated picking
511 using 2D reference in Relion and extracted with the box sizes of 320 pixels for the 44m Fab
512 bound 330 SOSIP Env trimer complexes. The extracted particles were imported to CryoSPARC
513 v4.5, and the rest of the processing was performed there. After four rounds of rigorous 2D
514 classification, 363,761 particles were selected from the best 2D classes with high-resolution
515 features of the Ab-bound complex. This dataset was divided into 4 classes for Ab initio

516 reconstruction with C3 symmetry. The class 04, with 118572 particles, had the best Ab-bound
517 features among all the classes (Figure S6). Therefore, we considered class 04 for non-uniform
518 refinement by imposing C3 symmetry. The resolution of the 3D map was estimated at FSC 0.143.
519 The local resolution estimation tool in cryoSPARC was used to determine local resolution. The
520 Alphafold model of AIIMS 330 env and 44m bnAb were used for atomic model building using
521 Phenix1.19.2 [95]. For model fitting, the Cryo-EM maps of 330 Env trimers were docked on ferritin
522 structure (PDB: 3BVE) symmetrically on four sites. Overviews of Cryo-EM data processing are
523 shown in S. Table S4. The atomic model fitting was done and visualized using ChimeraX [96].

524 **Immunizations**

525 The rabbit immunization studies were conducted at a contract research organization (CRO),
526 Liveon Biolabs Private Limited, Karnataka, India, under GLP-compliant conditions. Liveon
527 Biolabs is an AAALAC International-accredited facility and is registered with the CCSEA,
528 Government of India. Female, naive New Zealand White rabbits, aged 4 months and weighing
529 between 2.0–2.5 kg, were used for the study. The protocol for animal use was approved by the
530 Institutional Animal Ethics Committee (IAEC) of Liveon Biolabs (Approval No.: LBPL-IAEC-008-
531 01/2021; Study No.: LBPL/NG-1736 (EF)). Prior to housing, the experimental room underwent
532 fumigation for decontamination, and microbial load was assessed using the settle plate method.
533 The rabbits were kept in a temperature-controlled Environment (20 ± 3 °C) with relative
534 humidity ranging from 30–70%, a 12-hour light/dark cycle, 12–15 air changes per hour, and a
535 noise level below 80 dBs. Mortality and morbidity were monitored twice daily, while clinical
536 observations were conducted at least once per day throughout the study. Body weight
537 measurements were recorded for all animals prior to the administration of the test item on Day
538 1 and subsequently on a weekly basis (±1 day) during the treatment period. The gp140 SOSIP
539 and NFL Env immunogens (G1 and G2) were administered at a dose of 20 µg of trimers, or an
540 equivalent molar amount SOSIP-ferritin nanoparticles (25 µg) (G3) formulated with the AddaVax
541 adjuvant (1:1 v/v) (vac-adx-10, Invivogen). The placebo group (G4) received only adjuvant with
542 sterile 1XPBS. Doses were calculated based on the molecular weight of the protein peptides,
543 excluding glycans, as described elsewhere[60,60]. Blood samples were collected from rabbits at
544 weeks 0, 4, 6, 16, 20, and 22. Before blood collection from the marginal ear vein, a local
545 anaesthetic cream containing 4% lidocaine was applied for 5 minutes. The immunization
546 process, including bleeding protocols, caused minimal and brief pain or distress, with no

547 significant impact on animal health. At the end of the experimental period, the rabbits were
548 euthanized using a lethal dose of sodium thiopental. Complement-deactivated serum samples
549 were subsequently analysed for their binding reactivity and neutralization potential.

550 **HIV-1 pseudovirus generation**

551 The HIV-1 pseudoviruses were produced in HEK293T cells as described previously[97] by co-
552 transfecting the corresponding full HIV-1 gp160 Envelope plasmid and a pSG3ΔEnv backbone
553 plasmid. Briefly, 1 × $10^5$ cells in 2 mL complete DMEM (10% fetal bovine serum (FBS) (Gibco,
554 26140079 and 1% penicillin and streptomycin (Gibco, 15140-122) were seeded per well of a 6-
555 well cell culture plate (Costar, 3506) the day before transfection. For transfection, Envelope
556 (1.25 μg) and delta Envelope (pSG3ΔEnv backbone) plasmids (2.50 μg) were mixed in a 1:2 ratio
557 in Opti-MEM (Gibco, 31985062), with a final volume of 200 μL per well, and incubated for 5 min
558 at room temperature. Next, 3 μL of PEI-Max transfection reagent (Polysciences, 24765) (1
559 mg/mL) was added to this mixture before further incubation for 15 min at room temperature.
560 This mixture was then added dropwise to the HEK 293T cells supplemented with fresh complete
561 DMEM growth media and incubated at 37 °C for 48 h. Pseudoviruses were then harvested by
562 filtering cell supernatants with 0.45 μm sterile filters (mdi), aliquoted, and stored at −80 °C until
563 usage.

564

565 **HIV-1 Neutralization assay**

566 Neutralization assays were carried out using TZM-bl reporter cells which is described
567 elsewhere[98]. The autologous and heterologous NAb response of end point sera was measured in
568 TZM-bl cell neutralization assays. Neutralization was measured as a reduction in luciferase gene
569 expression after a single round of infection of TZM-bl cells (NIH AIDS Reagent Program) with
570 HIV-1 Env pseudoviruses. The $TCID_{50}$ of the HIV-1 pseudoviruses was calculated and 200 $TCID_{50}$
571 of the virus was used in the neutralization assays through incubation with three-fold serially
572 diluted rabbit sera starting at a 1:20 dilution. Next, freshly trypsinized TZM-bl cells in a complete
573 DMEM (10% fetal bovine serum (FBS) (Gibco, 26140079 and 1% penicillin and streptomycin
574 (Gibco, 15140-122) containing 50 μg/mL DEAE-dextran (Sigma, D9885) at $10^5$ cells/well were
575 added and the plates were incubated at 37 °C for 48 h. Virus controls (cells with HIV-1 virus

576 only) and cell controls (cells without virus and antibody) were included. MuLV was used as a
577 negative control. After the incubation of the plates for 48 h, luciferase activity was measured
578 using the Bright-Glow Luciferase Assay System (Promega, E2610). $ID_{50}$ for antibodies were
579 calculated from a dose–response curve fit with a non-linear function using GraphPad Prism 8
580 software (San Diego, CA, USA). All neutralization assays were repeated at least 2 times, and the
581 data shown are from representative experiments.

582 **Statistical analysis**

583 Statistical significance between groups and subgroups was assessed using the Mann–Whitney U
584 test, Student's t-test, and one-way analysis of variance for continuous variables. For
585 representative results, experiments was done in replicates or repeated twice. All statistical
586 analyses and plotting were performed using GraphPad Prism (version 8.0; La Jolla, CA, USA)

587 **FUNDING**

588 This study was funded by the Department of Biotechnology (DBT), India
589 (BT/PR39156/DRUG/134/91/2021, BT/PR30120/MED/29/1339/2018) grants awarded to K.L.
590 This work was also supported by Department of Science & Technology-FIST (SR/FST/LSII-
591 039/2015) and DBT-BUILDER Program (BT/INF/22/SP22844/2017) grants awarded to S.D. S.K.
592 is supported by the DBT-Wellcome Trust India Alliance Early Career Fellowship Grant
593 IA/E/18/1/504307. The funders played no role in the study design, data collection, analysis, or
594 interpretation, nor in the writing of the manuscript or the decision to publish the results.

595 **ACKNOWLEDGMENTS**

596 The authors express gratitude to Prof. R.W. Sanders for generously providing the PPI4
597 expression vector and the training provided to S.D.S as a part of his HIV-1 Trust Fellowship. We
598 are grateful to the NIH AIDS reagent program for providing the HIV-1 research reagents and the
599 Neutralizing Antibody Consortium(NAC), IAVI, USA for providing the HIV-1 neutralizing
600 antibodies donated by Michel Nussenzweig, Hermann Katinger, Mark Connors, James Robinson,
601 Dennis Burton, John Mascola, Peter Kwong, and William Olson. We appreciate the support of
602 Liveon Biolabs for conducting the immunization studies. We also extend our appreciation for the
603 IAVI-Leader Development Program awarded to S.D.S.

604 **AUTHOR CONTRIBUTIONS**

605 Conceptualization and implementation; S.D.S., S.Ku, and K.L., EM work & data acquisition; S.D.S.,
606 A.C., Formal analysis; S.D.S., S.Ku, K.L., S.D., Biophysical analysis; A.C., S.D.S., L.M., B.M., E.A.S.,
607 Expression and purifications: S.D.S., M.P., A.R., I.A., S.S., V.I., A.G., T.B., & R.Ku., ELISA &
608 neutralization assays; S.D.S., S.S, A.R., S.Ka, A.W.H., Animal studies; S.D.S., S.Ka, H.B., A.G., & A.W.H.
609 Octet experimentation; S.D.S., R.Ku., S.A., and M.P., Original manuscript writing; S.D.S., S.Ku, A.C.,
610 & K.L., Supervision; S.D., & K.L., Project administration; S.D.S. & S.Ku, funding acquisition; S.D., &
611 K.L. All authors have read and agreed to the published version of the manuscript.

612 **CONFLICT OF INTERESTS**

613 An Indian patent application (202211004612) has been filed on the 330 SOSIP Env trimer
614 described in this study. The following authors: K.L., S.D.S., S.Ku. and S.S. are listed as inventors on
615 the patent. The other authors declare no conflicts of interest.

616 **DATA AVAILABILITY**

617 The modified 330 Envelope protomer sequences have been deposited in GenBank under
618 accession numbers: PV575182 (330_SOSIP), PV575183 (330_NFL), and PV575184 (330_SOSIP
619 Ferritin Nanoparticle). The cryo-EM maps and atomic coordinates of the reported structures
620 have been deposited in the Electron Microscopy Data Bank (EMDB) and Protein Data Bank (PDB)
621 under accession codes EMD-66717 and 9XC1, respectively, for the 330 SOSIP Env trimer in
622 complex with bNAb 44m. Additional data are available from the corresponding authors upon
623 reasonable request.

624 **REFERENCES**


625 1. Burton, D. R. *et al.* A Blueprint for HIV Vaccine Discovery. *Cell Host Microbe* **12**, 396–407
626 (2012).
627 2. Simek, M. D. *et al.* Human Immunodeficiency Virus Type 1 Elite Neutralizers: Individuals with
628 Broad and Potent Neutralizing Activity Identified by Using a High-Throughput Neutralization
629 Assay together with an Analytical Selection Algorithm. *J. Virol.* **83**, 7337–7348 (2009).

630 3. van den Kerkhof, T. L. G. M. *et al.* Early development of broadly reactive HIV-1 neutralizing
631 activity in elite neutralizers. *AIDS* **28**, 1237 (2014).
632 4. Mascola, J. R. *et al.* Protection of macaques against vaginal transmission of a pathogenic HIV-
633 1/SIV chimeric virus by passive infusion of neutralizing antibodies. *Nat. Med.* **6**, 207–210
634 (2000).
635 5. Mascola, J. R. *et al.* Protection of Macaques against pathogenic simian/human
636 immunodeficiency virus 89.6PD by passive transfer of neutralizing antibodies. *J. Virol.* **73**,
637 4009–4018 (1999).
638 6. Parren, P. W. *et al.* Antibody protects macaques against vaginal challenge with a pathogenic
639 R5 simian/human immunodeficiency virus at serum levels giving complete neutralization in
640 vitro. *J. Virol.* **75**, 8340–8347 (2001).
641 7. Moldt, B. *et al.* Highly potent HIV-specific antibody neutralization in vitro translates into
642 effective protection against mucosal SHIV challenge in vivo. *Proc. Natl. Acad. Sci. U. S. A.* **109**,
643 18921–18925 (2012).
644 8. Hessell, A. J. *et al.* Broadly neutralizing human anti-HIV antibody 2G12 is effective in
645 protection against mucosal SHIV challenge even at low serum neutralizing titers. *PLoS*
646 *Pathog.* **5**, e1000433 (2009).
647 9. Karasavvas, N. *et al.* The Thai Phase III HIV Type 1 Vaccine Trial (RV144) Regimen Induces
648 Antibodies That Target Conserved Regions Within the V2 Loop of gp120. *AIDS Res. Hum.*
649 *Retroviruses* **28**, 1444–1457 (2012).
650 10. Kim, J., Excler, J.-L. & Michael, N. Lessons from the RV144 Thai Phase III HIV-1 Vaccine Trial
651 and the search for correlates of protection. *Annu. Rev. Med.* **66**, (2014).

652 11. Sanders, R. W. *et al.* A Next-Generation Cleaved, Soluble HIV-1 Env Trimer, BG505 SOSIP.664
653 gp140, Expresses Multiple Epitopes for Broadly Neutralizing but Not Non-Neutralizing
654 Antibodies. *PLOS Pathog.* **9**, e1003618 (2013).
655 12. Torrents de la Peña, A. *et al.* Improving the Immunogenicity of Native-like HIV-1 Envelope
656 Trimers by Hyperstabilization. *Cell Rep.* **20**, 1805–1817 (2017).
657 13. Torrents de la Peña, A. *et al.* Immunogenicity in Rabbits of HIV-1 SOSIP Trimers from Clades
658 A, B, and C, Given Individually, Sequentially, or in Combination. *J. Virol.* **92**, (2018).
659 14. Schorcht, A. *et al.* Neutralizing Antibody Responses Induced by HIV-1 Envelope Glycoprotein
660 SOSIP Trimers Derived from Elite Neutralizers. *J. Virol.* **94**, 10.1128/jvi.01214-20 (2020).
661 15. de Taeye, S. W. *et al.* Immunogenicity of Stabilized HIV-1 Envelope Trimers with Reduced
662 Exposure of Non-neutralizing Epitopes. *Cell* **163**, 1702–1715 (2015).
663 16. Sok, D. *et al.* Rapid elicitation of broadly neutralizing antibodies to HIV by immunization in
664 cows. *Nature* **548**, 108–111 (2017).
665 17. Sanders, R. W. *et al.* HIV-1 VACCINES. HIV-1 neutralizing antibodies induced by native-like
666 envelope trimers. *Science* **349**, aac4223 (2015).
667 18. Houser, K. V. *et al.* Safety and immunogenicity of an HIV-1 prefusion-stabilized envelope
668 trimer (Trimer 4571) vaccine in healthy adults: A first-in-human open-label, randomized,
669 dose-escalation, phase 1 clinical trial. *eClinicalMedicine* **48**, (2022).
670 19. Gartner, M. J., Roche, M., Churchill, M. J., Gorry, P. R. & Flynn, J. K. Understanding the
671 mechanisms driving the spread of subtype C HIV-1. *EBioMedicine* **53**, 102682 (2020).
672 20. Hemelaar, J., Gouws, E., Ghys, P. D. & Osmanov, S. Global and regional distribution of HIV-1
673 genetic subtypes and recombinants in 2004. *AIDS Lond. Engl.* **20**, W13-23 (2006).
674 21. Ahmed, S. *et al.* Stabilization of a soluble, native-like trimeric form of an efficiently cleaved
675 Indian HIV-1 clade C envelope glycoprotein. *J. Biol. Chem.* **292**, 8236–8243 (2017).

676 22. Rutten, L. *et al.* A Universal Approach to Optimize the Folding and Stability of Prefusion-
677 Closed HIV-1 Envelope Trimers. *Cell Rep.* **23**, 584–595 (2018).
678 23. Kumar, R. *et al.* Elicitation of potent serum neutralizing antibody responses in rabbits by
679 immunization with an HIV-1 clade C trimeric Env derived from an Indian elite neutralizer.
680 *PLOS Pathog.* **17**, e1008977 (2021).
681 24. Kumar, S. *et al.* Design and immunogenicity of an HIV-1 clade C pediatric envelope
682 glycoprotein stabilized by multiple platforms. *BioRxiv Prepr. Serv. Biol.* 2024.09.14.613016
683 (2024) doi:10.1101/2024.09.14.613016.
684 25. Schiller, J. & Chackerian, B. Why HIV Virions Have Low Numbers of Envelope Spikes:
685 Implications for Vaccine Development. *PLOS Pathog.* **10**, e1004254 (2014).
686 26. Zhao, Q., Li, S., Yu, H., Xia, N. & Modis, Y. Virus-like particle-based human vaccines: quality
687 assessment based on structural and functional properties. *Trends Biotechnol.* **31**, 654–663
688 (2013).
689 27. Ludwig, C. & Wagner, R. Virus-like particles-universal molecular toolboxes. *Curr. Opin.*
690 *Biotechnol.* **18**, 537–545 (2007).
691 28. Jennings, G. T. & Bachmann, M. F. The coming of age of virus-like particle vaccines. *Biol. Chem.*
692 **389**, 521–536 (2008).
693 29. Sliepen, K. *et al.* Presenting native-like HIV-1 envelope trimers on ferritin nanoparticles
694 improves their immunogenicity. *Retrovirology* **12**, 82 (2015).
695 30. He, L. *et al.* Presenting native-like trimeric HIV-1 antigens with self-assembling nanoparticles.
696 *Nat. Commun.* **7**, 12041 (2016).
697 31. Goo, L., Chohan, V., Nduati, R. & Overbaugh, J. Early development of broadly neutralizing
698 antibodies in HIV-1–infected infants. *Nat. Med.* **20**, 655–658 (2014).

699 32. Ditse, Z. *et al.* HIV-1 Subtype C-Infected Children with Exceptional Neutralization Breadth
700 Exhibit Polyclonal Responses Targeting Known Epitopes. *J. Virol.* **92**, (2018).
701 33. Kumar, S. *et al.* An HIV-1 Broadly Neutralizing Antibody from a Clade C-Infected Pediatric
702 Elite Neutralizer Potently Neutralizes the Contemporaneous and Autologous Evolving
703 Viruses. *J. Virol.* **93**, e01495-18 (2019).
704 34. Makhdoomi, M. A. *et al.* Neutralization resistant HIV-1 primary isolates from antiretroviral
705 naïve chronically infected children in India. *Virology* **499**, 105–113 (2016).
706 35. Mishra, N. *et al.* Viral Characteristics Associated with Maintenance of Elite Neutralizing
707 Activity in Chronically HIV-1 Clade C-Infected Monozygotic Pediatric Twins. *J. Virol.* **93**,
708 e00654-19, /jvi/93/17/JVI.00654-19.atom (2019).
709 36. Kumar, S. *et al.* Recognition determinants of improved HIV-1 neutralization by a heavy chain
710 matured pediatric antibody. *iScience* **26**, 107579 (2023).
711 37. Simonich, C. A. *et al.* HIV-1 Neutralizing Antibodies with Limited Hypermutation from an
712 Infant. *Cell* **166**, 77–87 (2016).
713 38. Sharma, S. K. *et al.* Cleavage-Independent HIV-1 Env Trimers Engineered as Soluble Native
714 Spike Mimetics for Vaccine Design. *Cell Rep.* **11**, 539–550 (2015).
715 39. Guenaga, J. *et al.* Structure-Guided Redesign Increases the Propensity of HIV Env To Generate
716 Highly Stable Soluble Trimers. *J. Virol.* **90**, 2806–2817 (2015).
717 40. Joyce, M. G. *et al.* Soluble Prefusion Closed DS-SOSIP.664-Env Trimers of Diverse HIV-1
718 Strains. *Cell Rep.* **21**, 2992–3002 (2017).
719 41. Kumar, S. *et al.* B cell repertoire sequencing of HIV-1 pediatric elite-neutralizers identifies
720 multiple broadly neutralizing antibody clonotypes. *Front. Immunol.* **15**, 1272493 (2024).
721 42. A Recombinant Human Immunodeficiency Virus Type 1 Envelope Glycoprotein Complex
722 Stabilized by an Intermolecular Disulfide Bond between the gp120 and gp41 Subunits Is an

723 Antigenic Mimic of the Trimeric Virion-Associated Structure | Journal of Virology.
724 https://journals.asm.org/doi/full/10.1128/JVI.74.2.627-643.2000.
725 43. Sanders, R. W. *et al.* Stabilization of the soluble, cleaved, trimeric form of the envelope
726 glycoprotein complex of human immunodeficiency virus type 1. *J. Virol.* **76**, 8875–8889
727 (2002).
728 44. Binley, J. M. *et al.* Enhancing the proteolytic maturation of human immunodeficiency virus
729 type 1 envelope glycoproteins. *J. Virol.* **76**, 2606–2616 (2002).
730 45. Ringe, R. P. *et al.* Improving the Expression and Purification of Soluble, Recombinant Native-
731 Like HIV-1 Envelope Glycoprotein Trimers by Targeted Sequence Changes. *J. Virol.* **91**,
732 (2017).
733 46. The Design and Immunogenicity of an HIV-1 Clade C Pediatric Envelope Glycoprotein
734 Stabilized by Multiple Platforms. https://www.mdpi.com/2076-393X/13/2/110.
735 47. Guenaga, J. *et al.* Glycine Substitution at Helix-to-Coil Transitions Facilitates the Structural
736 Determination of a Stabilized Subtype C HIV Envelope Glycoprotein. *Immunity* **46**, 792-
737 803.e3 (2017).
738 48. Rodrigues, M. Q., Alves, P. M. & Roldão, A. Functionalizing Ferritin Nanoparticles for Vaccine
739 Development. *Pharmaceutics* **13**, 1621 (2021).
740 49. López-Sagaseta, J., Malito, E., Rappuoli, R. & Bottomley, M. J. Self-assembling protein
741 nanoparticles in the design of vaccines. *Comput. Struct. Biotechnol. J.* **14**, 58–68 (2016).
742 50. Schommers, P. *et al.* Restriction of HIV-1 Escape by a Highly Broad and Potent Neutralizing
743 Antibody. *Cell* **180**, 471-489.e22 (2020).
744 51. Julien, J.-P. *et al.* Broadly Neutralizing Antibody PGT121 Allosterically Modulates CD4 Binding
745 via Recognition of the HIV-1 gp120 V3 Base and Multiple Surrounding Glycans. *PLoS Pathog.*
746 **9**, e1003342 (2013).

747 52. Kumar, S. *et al.* A $V_H$ 1-69 antibody lineage from an infected Chinese donor potently
748 neutralizes HIV-1 by targeting the V3 glycan supersite. *Sci. Adv.* **6**, eabb1328 (2020).
749 53. Barnes, C. O. *et al.* Structural characterization of a highly-potent V3-glycan broadly
750 neutralizing antibody bound to natively-glycosylated HIV-1 envelope. *Nat. Commun.* **9**, 1251
751 (2018).
752 54. Steichen, J. M. *et al.* A generalized HIV vaccine design strategy for priming of broadly
753 neutralizing antibody responses. *Science* **366**, eaax4380 (2019).
754 55. Saunders, K. O. *et al.* Targeted selection of HIV-specific antibody mutations by engineering B
755 cell maturation. *Science* **366**, eaay7199 (2019).
756 56. Simonich, C. A. *et al.* Kappa chain maturation helps drive rapid development of an infant HIV-
757 1 broadly neutralizing antibody lineage. *Nat. Commun.* **10**, 2190 (2019).
758 57. Guenaga, J. *et al.* Glycine Substitution at Helix-to-Coil Transitions Facilitates the Structural
759 Determination of a Stabilized Subtype C HIV Envelope Glycoprotein. *Immunity* **46**, 792-
760 803.e3 (2017).
761 58. Pancera, M. *et al.* Structure and immune recognition of trimeric pre-fusion HIV-1 Env. *Nature*
762 **514**, 455–461 (2014).
763 59. Behrens, A.-J. *et al.* Composition and Antigenic Effects of Individual Glycan Sites of a Trimeric
764 HIV-1 Envelope Glycoprotein. *Cell Rep.* **14**, 2695–2706 (2016).
765 60. Brouwer, P. J. M. *et al.* Immunofocusing and enhancing autologous Tier-2 HIV-1
766 neutralization by displaying Env trimers on two-component protein nanoparticles. *Npj*
767 *Vaccines* **6**, 1–14 (2021).
768 61. Ozorowski, G. *et al.* Effects of Adjuvants on HIV-1 Envelope Glycoprotein SOSIP Trimers *In*
769 *Vitro. J. Virol.* **92**, (2018).

770 62. Ahmed, S. *et al.* Enhancing anti-viral neutralization response to immunization with HIV-1
771 envelope glycoprotein immunogens. *Npj Vaccines* **8**, 1–10 (2023).
772 63. Sutar, J. *et al.* Geospatial HIV-1 subtype C gp120 sequence diversity and its predicted impact
773 on broadly neutralizing antibody sensitivity. *PLOS ONE* **16**, e0251969 (2021).
774 64. Ariën, K. K., Vanham, G. & Arts, E. J. Is HIV-1 evolving to a less virulent form in humans? *Nat.*
775 *Rev. Microbiol.* **5**, 141–151 (2007).
776 65. Taylor, B. S., Sobieszczyk, M. E., McCutchan, F. E. & Hammer, S. M. The challenge of HIV-1
777 subtype diversity. *N. Engl. J. Med.* **358**, 1590–1602 (2008).
778 66. Huang, A. *et al.* Global Comparison of Drug Resistance Mutations After First-Line
779 Antiretroviral Therapy Across Human Immunodeficiency Virus-1 Subtypes. *Open Forum*
780 *Infect. Dis.* **3**, ofv158 (2016).
781 67. Julien, J.-P. *et al.* Design and structure of two HIV-1 clade C SOSIP.664 trimers that increase
782 the arsenal of native-like Env immunogens. *Proc. Natl. Acad. Sci. U. S. A.* **112**, 11947–11952
783 (2015).
784 68. Kumar, S. *et al.* Neutralizing Antibodies Induced by First-Generation gp41-Stabilized HIV-1
785 Envelope Trimers and Nanoparticles. *mBio* **12**, 10.1128/mbio.00429-21 (2021).
786 69. Borst, A. J. *et al.* Germline VRC01 antibody recognition of a modified clade C HIV-1 envelope
787 trimer and a glycosylated HIV-1 gp120 core. *eLife* **7**, e37688 (2018).
788 70. Ringe, R. P. *et al.* Glycan heterogeneity as a cause of the persistent fraction in HIV-1
789 neutralization. *PLOS Pathog.* **19**, e1011601 (2023).
790 71. Xu, D. *et al.* Design of universal Ebola virus vaccine candidates via immunofocusing. *Proc.*
791 *Natl. Acad. Sci. U. S. A.* **121**, e2316960121.
792 72. Powell, A. E. *et al.* Multimerization of Ebola GPΔmucin on protein nanoparticle vaccines has
793 minimal effect on elicitation of neutralizing antibodies. *Front. Immunol.* **13**, 942897 (2022).

794 73. Casazza, J. P. *et al.* Phase 1 dose-escalation trial evaluating a group 2 influenza hemagglutinin
795 stabilized stem nanoparticle vaccine. *Npj Vaccines* **9**, 1–10 (2024).
796 74. Tang, P. *et al.* A ferritin nanoparticle vaccine based on the hemagglutinin extracellular
797 domain of swine influenza A (H1N1) virus elicits protective immune responses in mice and
798 pigs. *Front. Immunol.* **15**, (2024).
799 75. Stephens, L. M. & Varga, S. M. Nanoparticle vaccines against respiratory syncytial virus.
800 *Future Virol.* **15**, 763–778.
801 76. Swanson, K. A. *et al.* A respiratory syncytial virus (RSV) F protein nanoparticle vaccine
802 focuses antibody responses to a conserved neutralization domain. *Sci. Immunol.* **5**, eaba6466
803 (2020).
804 77. Joyce, M. G. *et al.* SARS-CoV-2 ferritin nanoparticle vaccines elicit broad SARS coronavirus
805 immunogenicity. *bioRxiv* 2021.05.09.443331 (2021) doi:10.1101/2021.05.09.443331.
806 78. Weidenbacher, P. A.-B. *et al.* A ferritin-based COVID-19 nanoparticle vaccine that elicits
807 robust, durable, broad-spectrum neutralizing antisera in non-human primates. *Nat. Commun.*
808 **14**, 2149 (2023).
809 79. Yu, J. *et al.* Ad26.COV2.S and SARS-CoV-2 spike protein ferritin nanoparticle vaccine protect
810 against SARS-CoV-2 Omicron BA.5 challenge in macaques. *Cell Rep. Med.* **4**, 101018 (2023).
811 80. Johnston, S. C. *et al.* A SARS-CoV-2 Spike Ferritin Nanoparticle Vaccine Is Protective and
812 Promotes a Strong Immunological Response in the Cynomolgus Macaque Coronavirus
813 Disease 2019 (COVID-19) Model. *Vaccines* **10**, 717 (2022).
814 81. Guenaga, J. *et al.* Structure-Guided Redesign Increases the Propensity of HIV Env To Generate
815 Highly Stable Soluble Trimers. *J. Virol.* **90**, 2806–2817 (2016).
816 82. Rappuoli, R., Bottomley, M., D'Oro, U., Finco, O. & Gregorio, E. Reverse vaccinology 2.0:
817 Human immunology instructs vaccine antigen design. *J. Exp. Med.* **213**, jem.20151960 (2016).

818 83. Klasse, P. J., Ozorowski, G., Sanders, R. W. & Moore, J. P. Env Exceptionalism: Why Are HIV-1
819 Env Glycoproteins Atypical Immunogens? *Cell Host Microbe* **27**, 507–518 (2020).
820 84. Seabright, G. E., Doores, K. J., Burton, D. R. & Crispin, M. Protein and Glycan Mimicry in HIV
821 Vaccine Design. *J. Mol. Biol.* **431**, 2223–2247 (2019).
822 85. Veneziano, R. *et al.* Role of nanoscale antigen organization on B-cell activation probed using
823 DNA origami. *Nat. Nanotechnol.* **15**, 716–723 (2020).
824 86. ACTS, RULES AND GUIDELINES: Committee for the Purpose of Control And Supervision of
825 Experiments on Animals.
826 https://ccsea.gov.in/Content/54_1_ACTS,RULESANDGUIDELINES.aspx.
827 87. Klasse, P. J. *et al.* Influences on trimerization and aggregation of soluble, cleaved HIV-1 SOSIP
828 envelope glycoprotein. *J. Virol.* **87**, 9873–9885 (2013).
829 88. de Taeye, S. W. *et al.* Immunogenicity of Stabilized HIV-1 Envelope Trimers with Reduced
830 Exposure of Non-neutralizing Epitopes. *Cell* **163**, 1702–1715 (2015).
831 89. Sok, D. *et al.* Recombinant HIV envelope trimer selects for quaternary-dependent antibodies
832 targeting the trimer apex. *Proc. Natl. Acad. Sci. U. S. A.* **111**, 17624–17629 (2014).
833 90. del Moral-Sánchez, I. *et al.* Triple tandem trimer immunogens for HIV-1 and influenza nucleic
834 acid-based vaccines. *Npj Vaccines* **9**, 1–18 (2024).
835 91. Kumar, S. *et al.* Recognition determinants of improved HIV-1 neutralization by a heavy chain
836 matured pediatric antibody. *iScience* **26**, 107579 (2023).
837 92. Tang, G. *et al.* EMAN2: An extensible image processing suite for electron microscopy. *J. Struct.*
838 *Biol.* **157**, 38–46 (2007).
839 93. Kumar, A., P., S., Gulati, S. & Dutta, S. User-friendly, High-throughput, and Fully Automated
840 Data Acquisition Software for Single-particle Cryo-electron Microscopy. *J. Vis. Exp.* 62832
841 (2021) doi:10.3791/62832.

842 94. Punjani, A., Rubinstein, J. L., Fleet, D. J. & Brubaker, M. A. cryoSPARC: algorithms for rapid
843 unsupervised cryo-EM structure determination. *Nat. Methods* **14**, 290–296 (2017).
844 95. Liebschner, D. *et al.* Macromolecular structure determination using X-rays, neutrons and
845 electrons: recent developments in Phenix. *Acta Crystallogr. Sect. Struct. Biol.* **75**, 861–877
846 (2019).
847 96. Goddard, T. D. *et al.* UCSF ChimeraX: Meeting modern challenges in visualization and
848 analysis. *Protein Sci. Publ. Protein Soc.* **27**, 14–25 (2018).
849 97. Mishra, N. *et al.* Broadly neutralizing plasma antibodies effective against autologous
850 circulating viruses in infants with multivariant HIV-1 infection. *Nat. Commun.* **11**, 4409
851 (2020).
852 98. Montefiori, D. C. Measuring HIV Neutralization in a Luciferase Reporter Gene Assay. in *HIV*
853 *Protocols* (eds. Prasad, V. R. & Kalpana, G. V.) 395–405 (Humana Press, Totowa, NJ, 2009).
854 doi:10.1007/978-1-59745-170-3_26.
855
856
857
858
859
860
861
862
863
864
865
866
867
868

869 **FIGURE LEGENDS:**

870

871 **Figure 1: Design & biochemical characterization of 330 gp140 Env trimers and ferritin**
872 **nanoparticles.** Linear representation of three 330 Envelope variants **(A)** Design of SOSIP with
873 the SOS-bond (A605-T605C), IP (I559P) stabilizing mutation along with TD8 mutations, a
874 intraprotomer disulfide bond (I201C-A433C), an improved furin cleavage (R6) with CD5 Signal
875 Peptide (SP) and Twin Strep-Tag (tst) tag **(B)** Design of NFL covalently linking gp120 to gp41
876 with flexible glycine serine (GGGGSGGGGS) linker **(C)** Design of H. pylori ferritin nanoparticle
877 linked glycine serine linker to SOSIP construct **(D)** A surface structure highlighting the TD8
878 stabilizing mutations (right) in the 330 Envelope construct. Structure was illustrated using
879 PyMOL and based on the BG505 SOSIP.664 crystal structure (PDB ID: 4ZMJ) **(E)** Size-exclusion
880 chromatography (SEC) profiles of AIIMS 330 Env trimers (SOSIP and NFL) and Ferritin
881 nanoparticles (NPs), eluted between 8–12 mL on a Superdex 200 Increase 10/300 GL column **(F)**
882 Negative Stain-EM 2-D class averages of NFL & SOSIP gp140 Env trimers and ferritin
883 nanoparticles **(G)** Guided by NS-TEM 2D class averages, four SOSIP gp140 Env trimers were
884 manually placed onto the multivalent ferritin nanoparticle using ChimeraX to produce a 3D
885 representation of the complex **(H)** Melting curve around 74°C of AIIMS 330 Envelope

886 **Figure 2: Antigenicity of 330 gp140 Env trimers and ferritin nanoparticles to HIV-1 bNAbs**
887 **and non-NAbs.** Representative AIIMS 330 Env binding curves with conformational specific
888 bNAbs (PGT145, CAP256.25, PGDM1400, PGT151), CD4 specific bNAbs (VRC01, N6), V3
889 Supersite (10.1074, AIIMS P01) along with non-nAbs (17b+sCD4, F105, A32, 48d) assessed by
890 ELISA.

891 **Figure 3: Octet sensograms kinetics of 330 Env to HIV-1 bNAbs and non-NAbs. (B)** Octet
892 Sensograms showing response shift (nm) over time (sec) of AIIMS 330 Env trimers and particles
893 with varied concentrations (500 nM, 166.6 nM, 55.5 nM, 18.5 nM, 6.1 nM) against the quaternary
894 specific bNAbs PGT145, PGD1400, cleavage dependent bNAb PGT151 and the non-nAbs F105 &
895 17b+sCD4.

896 **Figure 4: Structural and glycan homology of 330 SOSIP with BG505 & 16055 trimers (A-B)**
897 Atomic model comparison of 330 SOSIP Env trimer with BG505 SOSIP (PDB: 4TVP) (RMSD
898 gp120: 0.685 $A^0$, gp41: 0.478 $A^0$) **(C-D)** 16055 NFL (PDB: 5UM8) (RMSD gp120: 0.798 $A^0$, gp41:

899 0.739 $A^0$) SOSIP trimer. Colour coding of SOSIP trimers corresponding to segmented EM
900 densities are: dodger blue, AIIMS 330 SOSIP, deep pink, BG505 SOSIP and 16055. Within each
901 protomer, gp120 regions are highlighted in blue and pink, while gp41 regions are shown in
902 yellow and green **(E)** Presence of glycan hole in 330 Env at position 130, 295, 339 in HXB2
903 reference coordinates showed in top, front & side view **(F)** Figure depicting the total protein
904 accessible area across cross-clade Envelopes **(G)** Presence of total 28 PNGS in AIIMS 330 &
905 BG505 Envelope. An N indicates the presence of a PNGS, if NXT/S motif in a.a sequence whereas
906 X should not be proline. The glycan structure and alignment created by N-Glycosite tool from Los
907 Alamos HIV-1 sequence database.

908 **Figure 5: Cryo-EM structure of 330 SOSIP Env trimer in complex with autologous bNAb**
909 **AIIMS 44m (A)** Top and side views of Cryo-EM reconstructed map of AIIMS 330 SOSIP Env
910 trimer in complex with 44m bNAb. Colour coding corresponding to segmented EM densities are:
911 deep pink, 44m bNAb; dodger blue, gp120; golden rod, gp41 **(B)** The corresponding atomic
912 model fitted in the EM map (in gray) of AIIMS 330 SOSIP trimer in complex with 44m bNAb. The
913 model illustrates that three 44m bNAbs bind to each gp120 monomeric subunit, facilitating
914 effective neutralization **(C)** Atomic model of AIIMS 330 SOSIP trimer in complex with three 44m
915 bNAbs. **(D)** Atomic model of one protomer of gp120 binding to one 44m bnAb **(E)** Location of
916 CDRH and FR3 regions are shown here in different colours (CDRH1- cyan, CDRH2- deep green,
917 CDRH3- light green, FR3- light brown) **(F)** Key interacting residues AIIMS 44m bNAb - S30, Y52,
918 Y53, R78 and R109 highlighted in heteroatom colour, and corresponding interacting residues of
919 gp120 loops - E293, D325, R327, H330, N332, K337 and K446 highlighted in heteroatom colour
920 **(G)** Electrostatic surface potential map of 44m bnAb showing interaction of residues from gp120
921 loops with charged portion of 44m bnAb **(H)** The N-glycans N301, N332, N397, N442, and N448
922 located at the junction of AIIMS 44m bNAb and AIIMS 330 gp120 protomers.

923 **Figure 6: Immunogenicity & Neutralizing potential of 330 SOSIP, NFL Env trimers &**
924 **Ferritin NP's in NZW rabbits. (A)** Rabbit immunization Schedule. Four groups of rabbits were
925 immunized at week 0 (prime), 4 & 20 (boost), gp140 SOSIP and NFL Env immunogens (G1 and
926 G2) were administered at a dose of 20 μg of trimers, or an equivalent molar amount SOSIP-
927 ferritin nanoparticles (25 μg) (G3) formulated with the AddaVax adjuvant (1:1 v/v). Sera was
928 obtained at indicated intervals of week 4, 6, 8, 12, 16, 20 & 22 (red arrows). **(B)** Binding
929 endpoint titers (OD at A450) over time against autologous virus (330.16.E6) Dots and error bars

930 represent the median binding titers and standard deviations. The assay cut-off is marked with a
931 dotted line **(C)** Midpoint neutralization titers ($ID_{50}$) for week 22 sera of the immunized rabbits
932 against autologous (330.16.E6) and closely related (329.14.B1), and heterologous clade C
933 (MW965.26 and 25925) and Tier 1 clade B (SF162) pseudoviruses. Median ID50 titers NFL,
934 SOSIP & Ferritin NP group was 375, 830 & 1160. Statistical analysis was done using an unpaired
935 two-tailed Student's t-test and the assay cut-off is marked with a dotted line.

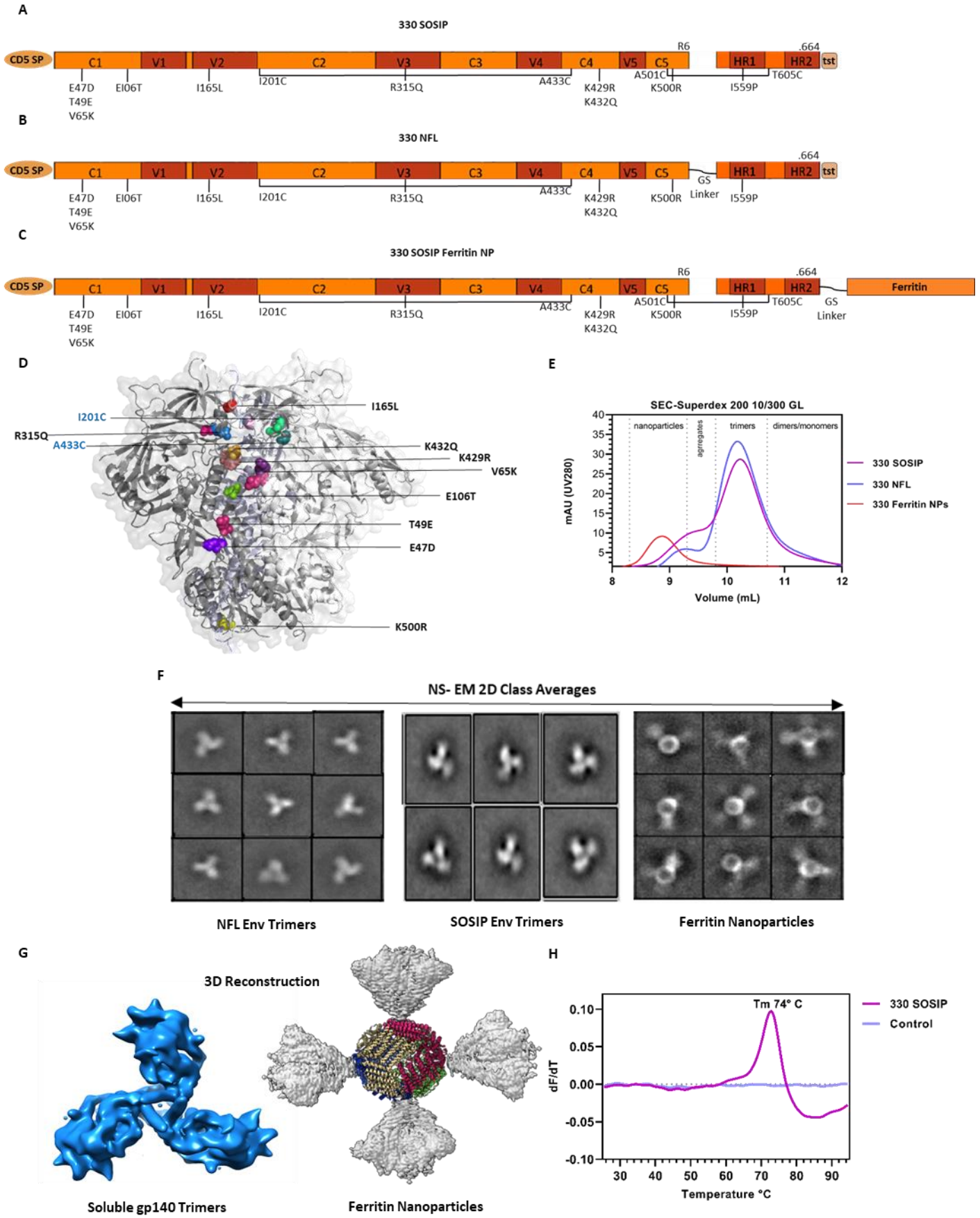
A
330 SOSIP
CD5 SP
C1
V1
V2
C2
V3
C3
V4
C4
V5
C5
R6
HR1
HR2
.664
tst
E47D
T49E
V65K
EI06T
I165L
I201C
R315Q
A433C
K429R
K432Q
A501C
K500R
T605C
I559P
B
330 NFL
GS
Linker
C
330 SOSIP Ferritin NP
Ferritin
D
I165L
I201C
R315Q
A433C
K432Q
K429R
V65K
E106T
T49E
E47D
K500R
E
SEC-Superdex 200 10/300 GL
nanoparticles
aggregates
trimers
dimers/monomers
mAU (UV280)
Volume (mL)
330 SOSIP
330 NFL
330 Ferritin NPs
F
NS- EM 2D Class Averages
NFL Env Trimers
SOSIP Env Trimers
Ferritin Nanoparticles
G
3D Reconstruction
Soluble gp140 Trimers
Ferritin Nanoparticles
H
Tm 74° C
dF/dT
Temperature °C
330 SOSIP
Control

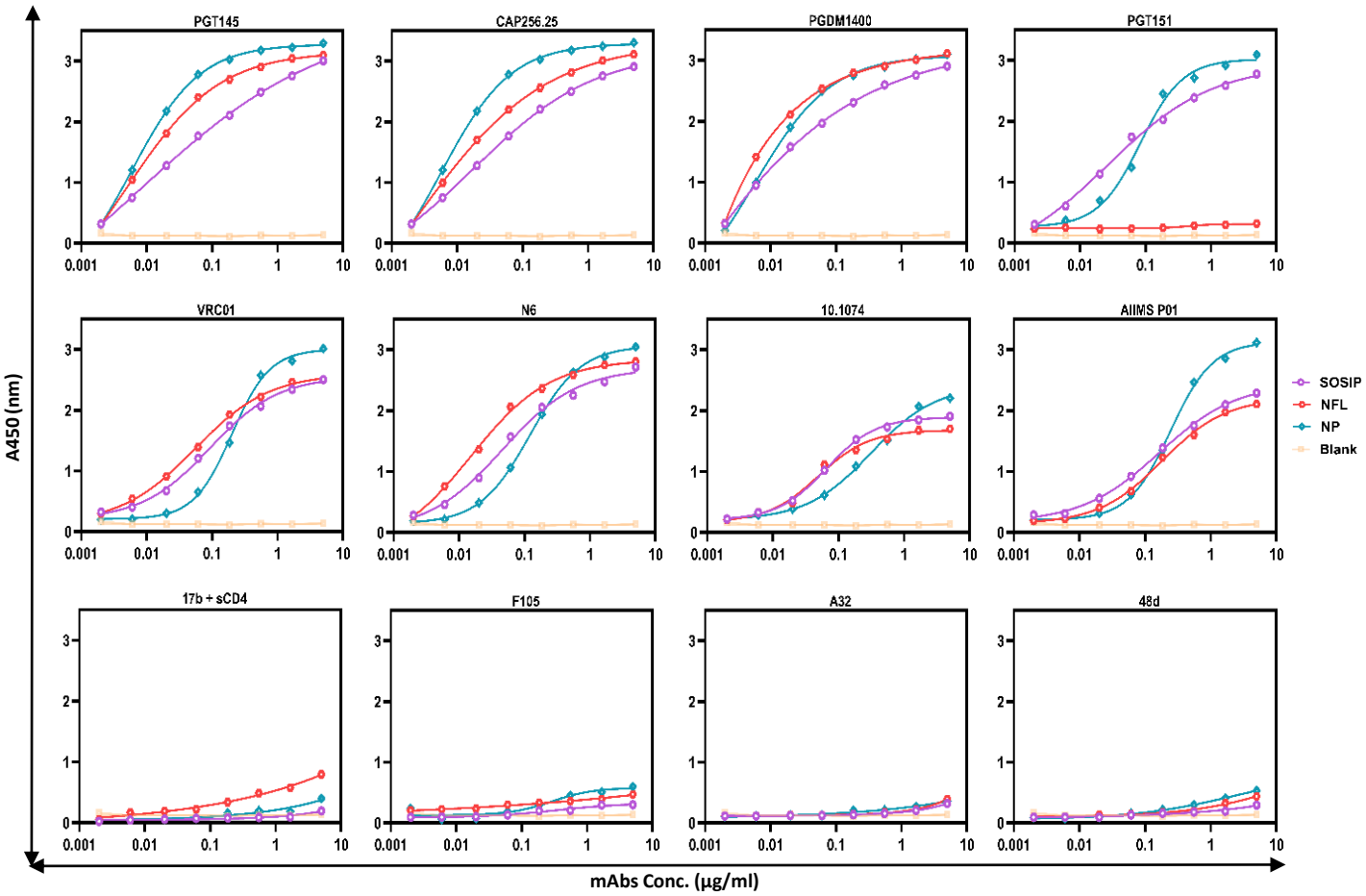
PGT145
CAP256.25
PGDM1400
PGT151
VRC01
N6
10.1074
AIIMS P01
17b + sCD4
F105
A32
48d
A450 (nm)
mAbs Conc. (µg/ml)
SOSIP
NFL
NP
Blank

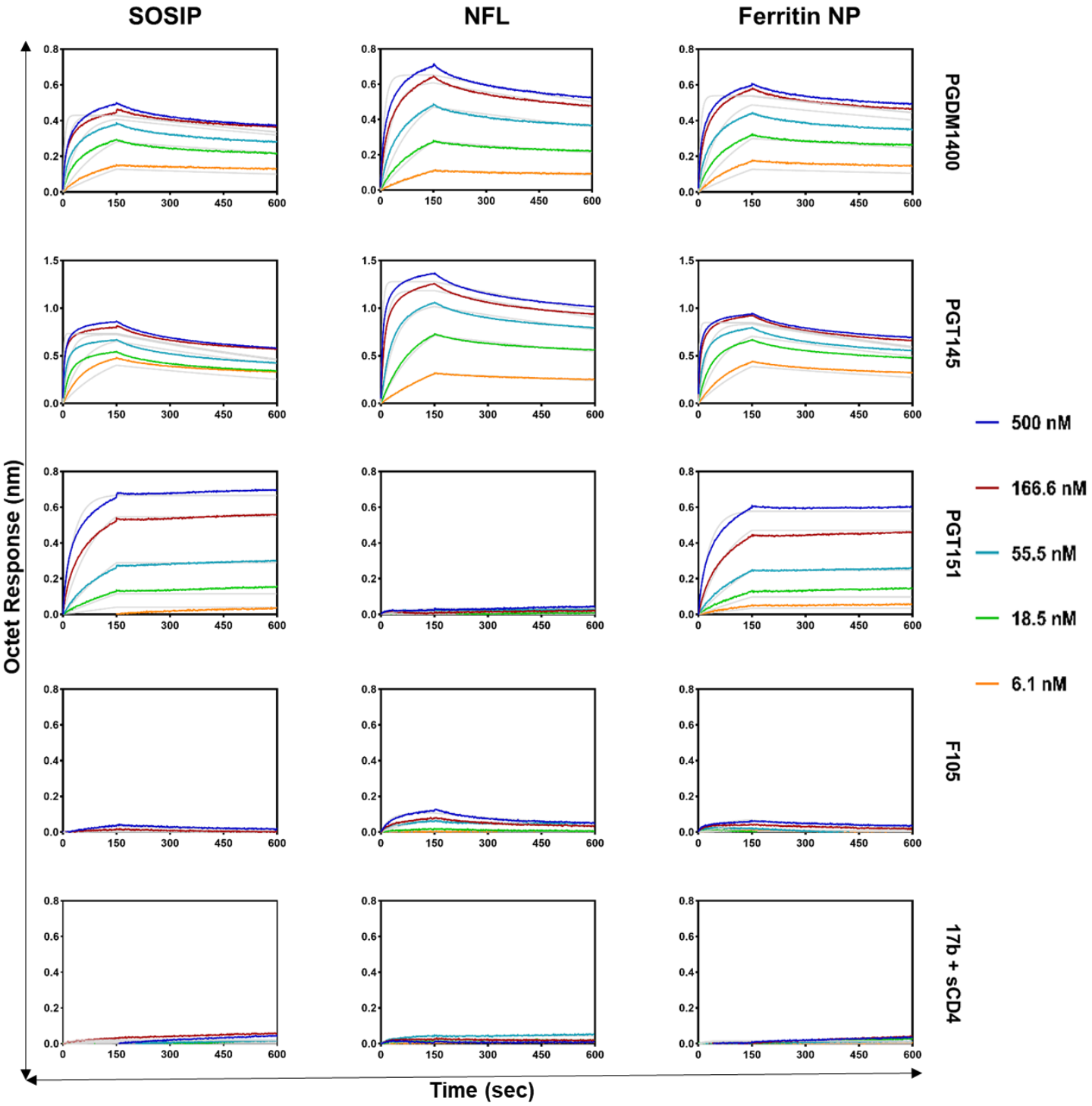
SOSIP
NFL
Ferritin NP
PGDM1400
PGT145
PGT151
F105
17b + sCD4
Octet Response (nm)
Time (sec)
500 nM
166.6 nM
55.5 nM
18.5 nM
6.1 nM

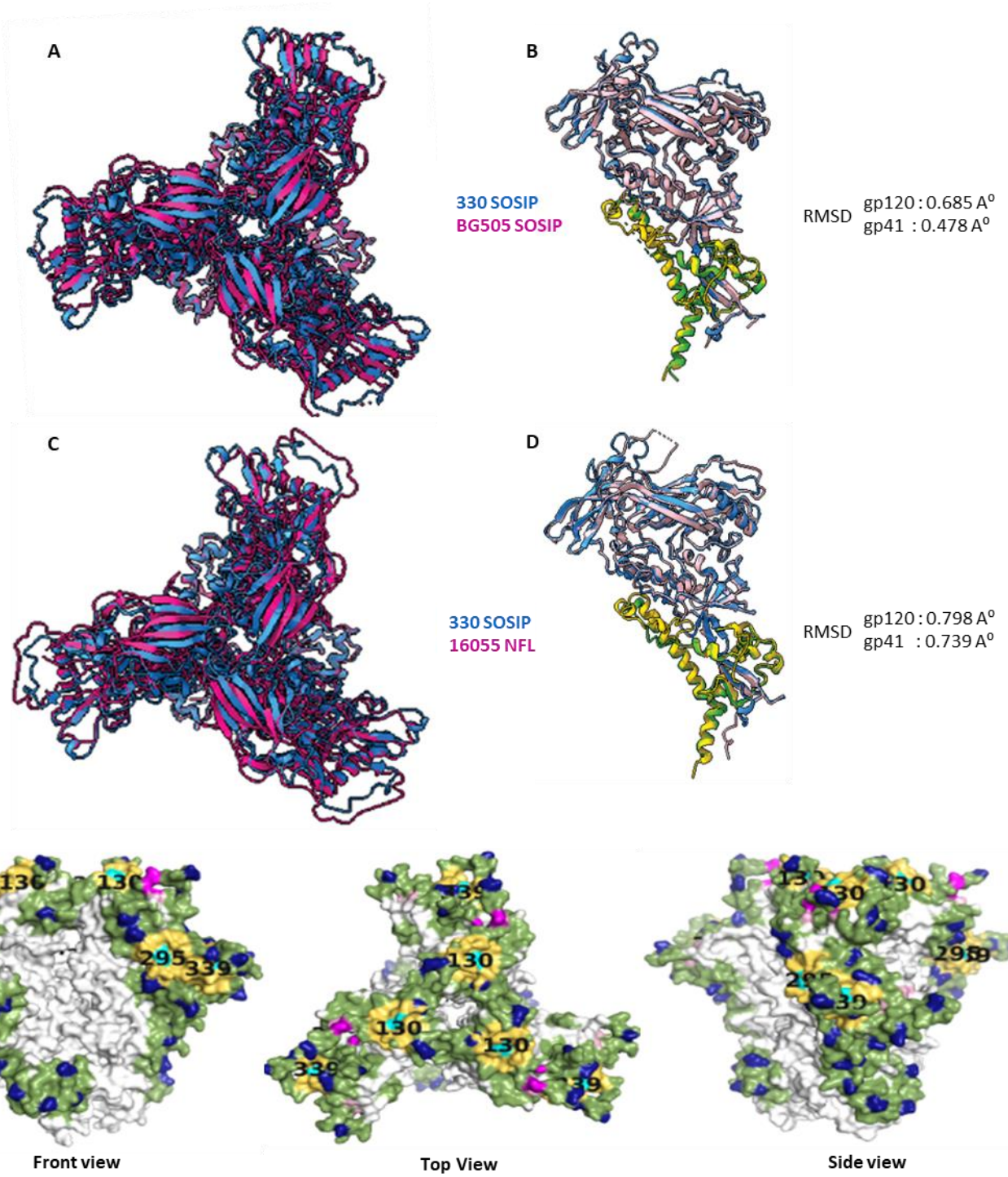
A
B
330 SOSIP
BG505 SOSIP
RMSD
gp120 : 0.685 A°
gp41 : 0.478 A°
C
D
330 SOSIP
16055 NFL
RMSD
gp120 : 0.798 A°
gp41 : 0.739 A°
E
295
339
130
Front view
Top View
Side view

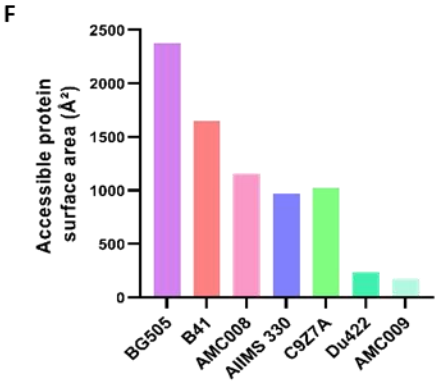
F
Accessible protein surface area (Å²)
2500
2000
1500
1000
500
0
BG505
B41
AMC008
AIIMS 330
C9Z7A
Du422
AMC009

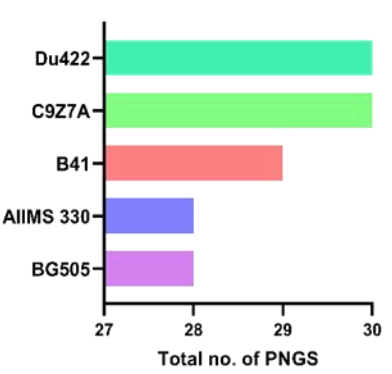
G
Du422
C9Z7A
B41
AIIMS 330
BG505
27
28
29
30
Total no. of PNGS

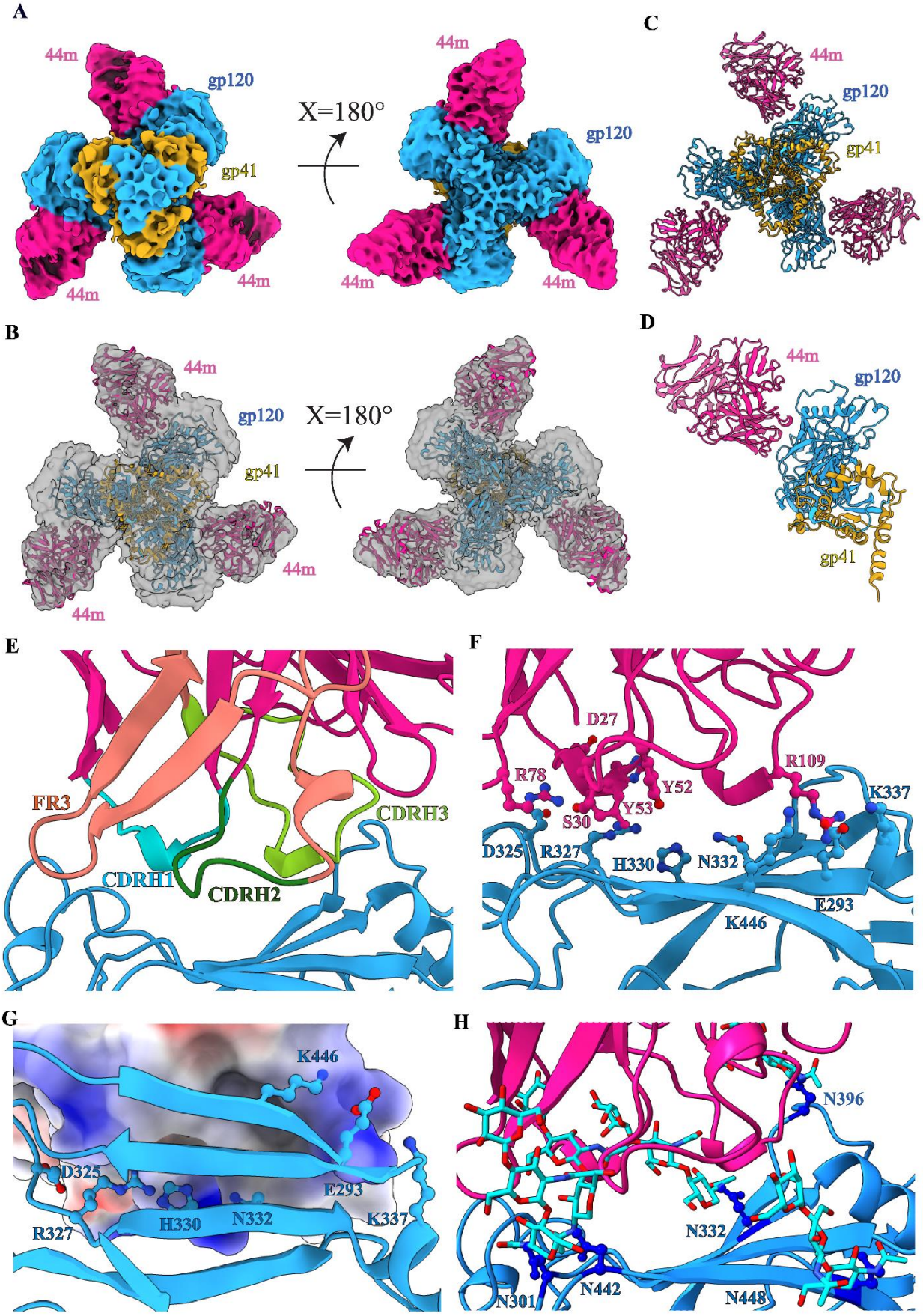
A
44m
gp120
gp41
44m
44m
X=180°
44m
gp120
44m
44m
C
44m
gp120
gp41
B
44m
gp120
gp41
44m
44m
X=180°
D
44m
gp120
gp41
E
FR3
CDRH1
CDRH2
CDRH3
F
D27
R78
Y52
Y53
S30
R109
K337
D325
R327
H330
N332
E293
K446
G
K446
D325
E293
R327
H330
N332
K337
H
N396
N332
N301
N442
N448

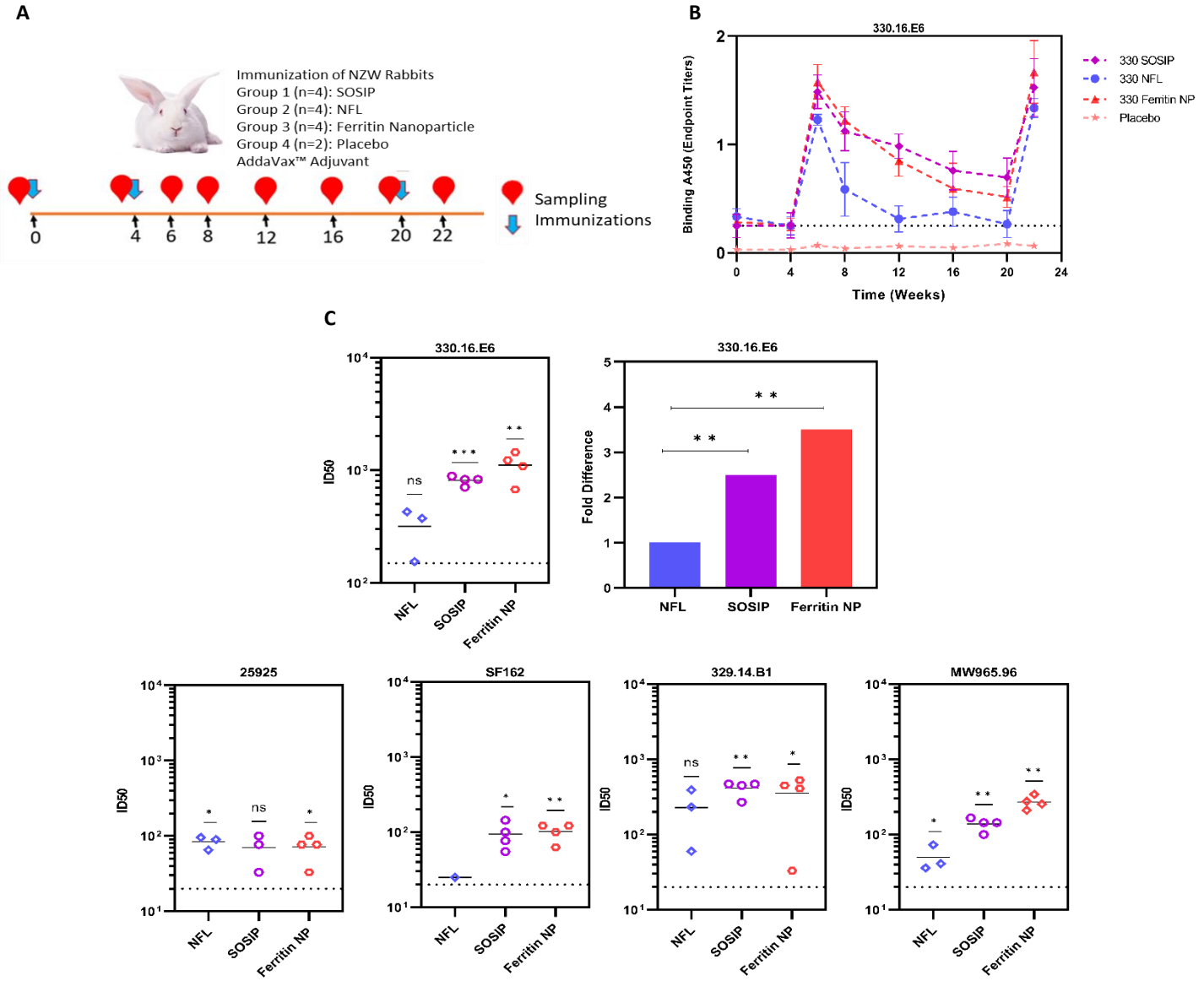
A
Immunization of NZW Rabbits
Group 1 (n=4): SOSIP
Group 2 (n=4): NFL
Group 3 (n=4): Ferritin Nanoparticle
Group 4 (n=2): Placebo
AddaVax™ Adjuvant
0
4
6
8
12
16
20
22
Sampling
Immunizations
B
330.16.E6
Binding A450 (Endpoint Titers)
Time (Weeks)
330 SOSIP
330 NFL
330 Ferritin NP
Placebo
C
330.16.E6
ID50
ns
* * *
* *
NFL
SOSIP
Ferritin NP
330.16.E6
Fold Difference
* *
* *
25925
SF162
329.14.B1
MW965.96